Cell Tissue Res (2009) 338:355–375
DOI 10.1007/s00441-009-0880-0

REGULAR ARTICLE

Ectopic synaptic ribbons in dendrites of mouse retinal ON- and OFF-bipolar cells

Masaaki Ishii · Katsuko Morigiwa · Motoharu Takao · Shigetada Nakanishi · Yutaka Fukuda · Osamu Mimura · Yoshihiko Tsukamoto

Received: 17 July 2009 / Accepted: 8 September 2009 / Published online: 27 October 2009

Abstract The ectopic distribution of synaptic ribbons in dendrites of mouse retinal bipolar cells was examined by using genetic ablation of metabotropic glutamate receptor subtype 6 (mGluR6), electron microscopy, and immunocytochemistry. Ectopic ribbons were observed in dendrites of rod and ON-cone bipolar cells in the mGluR6-deficient mouse but not in those of wild-type mice. The number of rod spherules facing the ectopic ribbons in mGluR6-deficient rod bipolar dendrites increased gradually during early growth and reached a plateau level of about 20% at 12 weeks. These ectopic ribbons were immunopositive for RIBEYE, a ribbon-specific protein, but the associated vesicles were immunonegative for synaptophysin, a synaptic-vesicle-specific protein. The presence of ectopic ribbons was correlated with an increase in the roundness of the invaginating dendrites of the rod bipolar cells. We further confirmed ectopic ribbons in dendrites of OFF-cone bipolar cells in wild-type retinas. Of the four types of OFF-cone bipolar cells (T1–T4), only the T2-type, which had a greater number of synaptic ribbons at the axon terminal and a thicker axon cylinder than the other types, had ectopic ribbons. Light-adapted experiments revealed that, in wild-type mice under enhanced-light adaptation (considered similar to the mGluR6-deficient state), the roundness in the invaginating dendrites and axon terminals of rod bipolar cells increased, but no ectopic ribbons were detected. Based on these findings and known mechanisms for neurotransmitter release and protein trafficking, the possible mechanisms underlying the ectopic ribbons are discussed on the basis of intracellular transport for the replenishment of synaptic proteins.

Keywords Retina · Ribbon synapse · Glutamate receptor · Neuronal polarity · Protein trafficking · Mouse (C57BL/6 J)

This study was partly supported by the Strategic Promotion System for Brain Science from the Science and Technology Agency of Japan (K.M.), Grant-in-Aid from the Japan Society for the Promotion of Science (12878144 to Y.T.), and Grant-in-Aid for Researchers, Hyogo College of Medicine (Y.T.).

M. Ishii · Y. Tsukamoto (✉)
Department of Biology, Hyogo College of Medicine,
Nishinomiya, Hyogo 663-8501, Japan
e-mail: ytsuka@hyo-med.ac.jp

M. Ishii · O. Mimura
Department of Ophthalmology, Hyogo College of Medicine,
Nishinomiya, Hyogo 663-8501, Japan

K. Morigiwa
EW89 Synchronicity Research Institute,
Tokyo 103-0027, Japan

M. Takao
Department of Human and Information Science, Tokai University,
Hiratsuka, Kanagawa 259-1292, Japan

S. Nakanishi
Osaka Bioscience Institute,
Suita, Osaka 565-0874, Japan

Y. Fukuda
Department of Physiology,
Osaka University Graduate School of Medicine,
Suita, Osaka 565-0871, Japan

Introduction

Synaptic ribbons have attracted the interest of many researchers over several decades because of their unique ultrastructure and functional importance (Vollrath and Spiwoks-Becker 1996; Wagner 1997; Sterling and Matthews 2005; tom Dieck and Brandstätter 2006). The synaptic ribbons of retinal bipolar cells are generally accepted as

being located at presynaptic sites of axon terminals. However, during the course of electron-microscopic studies of the retina of metabotropic glutamate receptor subtype 6 (mGluR6)-deficient mice, we have encountered ectopic synaptic ribbons in the dendrites of (ON-type) rod bipolar cells (Tsukamoto et al. 1999). We have also found, in these mGluR6-deficient mice, immunoreactivity for mGluR7, which is usually located at axon terminals of cone bipolar cells, in the dendrites of ON-cone bipolar cells (Tsukamoto et al. 2007). Intrigued by these findings, we have investigated the fine structures of ectopic ribbons, their development during early growth, and their immunoreactivity for ribbon-synapse-specific proteins in mGluR6-deficient rod bipolar cells by using both electron microscopy and immunocytochemistry.

However, ectopic ribbons are not uniquely found in ON-type bipolar cells of mGluR6-deficient mice. Kolb (1977) has previously indicated the occasional presence of synaptic ribbons in bipolar cell dendrites of cat retinas. More recently, Spiwoks-Becker et al. (2000) have confirmed the presence of these ectopic synaptic ribbons in cattle and mouse retinas and suggested that they are located in the dendrites of OFF-cone bipolar cells. We have now comprehensively studied wild-type retinas by using three-dimensional reconstruction in order to determine which of the four types of OFF-cone bipolar cells have ectopic ribbons and additionally to compare their morphological features.

For an in-depth investigation of these two cases of dendritic distribution of ectopic ribbons in mGluR6-deficient ON-type bipolar and OFF-cone bipolar cells, we have taken note of the correlation between the morphological changes and the presence of the ectopic ribbons that we have observed in mGluR6-deficient rod bipolar cells. Behrens et al. (1998) have demonstrated the adaptation-dependent morphological changes in rod bipolar axon terminals in rat retinas. On the other hand, Spiwoks-Becker et al. (2000) have reported that, in OFF-bipolar dendrites of mouse retinas, the presence of ectopic ribbons is modulated by daily light-dark adaptation. Based on these findings, we have analyzed the morphological changes in dendrites and axon terminals of rod bipolar cells and the presence of ectopic ribbons under dark, room-light, and "enhanced-light" adaptations in both wild-type and mGluR6-deficient mouse retinas. Our hypothesis is that the rod bipolar cells in the wild-type retina exposed to intense illumination (= enhanced-light-adapted state) simulate the mGluR6-deficient state with virtually null glutamate input.

Here, we report three major aspects of ectopic ribbons in the following order: first, a detailed description of ectopic ribbons in rod bipolar cells by using electron and confocal-fluorescence microscopy; second, the morphological characterization of the OFF-cone bipolar cells that have ectopic ribbons; third, the possible relationship of light conditioning and the presence/non-presence of ectopic ribbons in association with the changes in the shape of rod bipolar cells. Based on our findings, we discuss the differences in the ectopic ribbon phenomena between OFF-type and mGluR6-deficient ON-type bipolar cells and their possible common underlying mechanisms.

Materials and methods

Animals

For morphological studies, radial retinal sections were obtained from fifty commercially available, wild-type mice (C57BL/6 J, ~10 weeks old; CLEA Japan, Tokyo, Japan). Reconstruction and measurements of bipolar cells were performed by using 366 radial sections from electron micrographs of a wild-type mouse retina (C57BL/6 J, 9 weeks old) used in a previous study (Tsukamoto et al. 2001). Retinas were also obtained from thirty mGluR6-deficient (−/−) and thirty wild-type (+/+) mice (hybrid of 129/SvJ x C57Bl/6 J) bred as reported previously (Masu et al. 1995; Tagawa et al. 1999). The survival longevity of mGluR6-deficient mice was similar to that of wild-type mice. Experiments were carried out in compliance with the Guide for the Care and Use of Experimental Animals of Hyogo College of Medicine. Pieces of $G\alpha_o$-deficient retinas embedded in resin (Dhingra et al. 2000) were generously provided by Dr. N. Vardi, University of Pennsylvania, USA.

Electron microscopy of serial sections

Mice were deeply anesthetized with sodium pentobarbital (45 mg/kg, i.p.) before perfusion with 4% paraformaldehyde and 1% glutaraldehyde in cacodylate buffer, pH 7.4 (Sigma-Aldrich Japan, Tokyo, Japan). Pieces of the posterior retina were excised and immersed in 2% paraformaldehyde and 3% glutaraldehyde in cacodylate buffer, pH 7.4, microwave-irradiated for 10 min, and then left for 3 h at room temperature or overnight at 4°C. Tissue was post-fixed with 2% osmium tetroxide for 1 h at room temperature, stained *en bloc* with 3% uranyl acetate in 80% methanol, dehydrated with ethanol, and embedded in Araldite (Nisshin EM, Tokyo, Japan).

Retinas of 3-, 4-, 12-, and 90-week-old mGluR6-deficient and wild-type mice and of 10-week-old wild-type mice (C57BL/6 J) were sectioned serially for electron microscopy. Retinas were taken from mice under room-light, dark, or enhanced-light adaptation. To examine the rod spherules and cone pedicles, approximately 100

tangential serial sections (90 nm) were taken from the outer plexiform layer (OPL) of each retina (n=3 mice at each age and light adaptation). Sections were mounted on Formvar-covered slot grids, stained with uranyl acetate and lead citrate, and photographed at magnifications of ×1000 or ×3000 by using a JEM1220 electron microscope (JEOL, Tokyo). Selected synaptic areas were re-photographed at magnifications of ×20,000 or ×40,000.

Antibodies

A rabbit polyclonal antibody was raised against amino acids 971–985 (QPTKHGDNREHPNEQ) from the C-terminus of the B-domain of the ribbon-specific rat RIBEYE protein (Peptide Institute, Osaka, Japan), a peptide sequence identical to the transcription factor C-terminal binding protein 2 (CtBP2) sequence (Schmitz et al. 2000). This anti-RIBEYE B-domain antibody was used for Western blotting (Fig. 1a) and for immunohistochemical labeling of light-microscopic (Fig. 1b, d; see also below) and electron-microscopic images. As a control for labeling specificity, the antibody was also pre-mixed with antigen before immunolabeling the sections (no immunolabeling observed; Fig. 1c). The anti-RIBEYE B-domain antibody recognized two protein bands (Fig. 1a, double arrow) in the mouse retina as seen in a previous study (tom Dieck et al. 2005). In addition, the antibody detected CtBP2 protein (50 kDa) in both brain and retina protein samples. In the retinal blots, the low abundance protein band (Fig. 1a, asterisk) above the CtBP2 band was considered to be nicotinamide adenine dinucleotide^{+}-CtBP2 (Schmitz et al. 2000), whereas the bands below the CtBP2 band (Fig. 1a, double asterisk) were probably proteolytic breakdown products, as the B-domain of RIBEYE is known to be highly sensitive to proteolysis (Schmitz et al. 2000).

Mouse monoclonal anti-synaptophysin antibody was commercially obtained (1.0 mg/ml, clone number SY38; Millipore, Billerica, Mass., USA). This antibody stains a single band (38 kDa) on Western blots (Fig. 1a). Anti-synaptophysin staining of the retinal sections resulted in a pattern of synaptophysin immunoreactivity (see bleow) that was identical to that observed in a previous study (Wiedenmann and Franke 1985).

Rabbit polyclonal anti-protein kinase C-α (PKCα) antibody (59 mg/ml; Sigma-Aldrich Japan, Tokyo, Japan) was raised against amino acids 659–672 of rat PKCα. According to the manufacturer, this antibody stains a single band (80 kDa) on Western blots. Anti-PKCα staining of

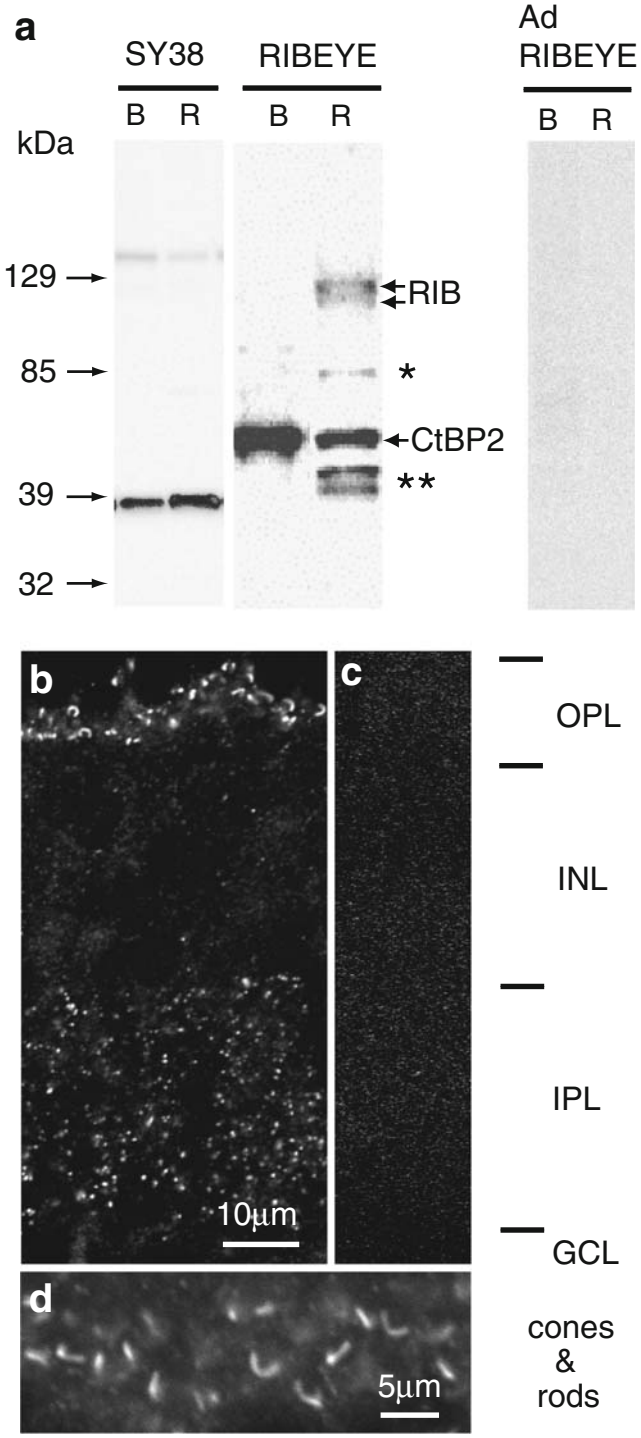

Fig. 1 Antibody characterization. **a** Western blot analysis of mouse brain (*B*) and retina (*R*) homogenates probed with anti-synaptophysin and anti-RIBEYE B-domain. In the mouse retina, immunopositive bands were detected for synaptophysin (*SY38*, 38 kDa) and RIBEYE B-domain (*RIBEYE*, ~110 kDa and 120 kDa). Pre-incubation of the anti-RIBEYE B-domain antibody with RIBEYE B-domain antigen blocked immunodetection of RIBEYE B-domain (*Ad RIBEYE*). **b** Vertical cryosections of mouse retina showing anti-RIBEYE B-domain immunoreactivity of photoreceptor ribbons in the outer plexiform layer (*OPL*) and bipolar cell ribbons in the inner plexiform layer (*IPL*). *INL* Inner nuclear layer, *GCL* ganglion cell layer. **c** Pre-incubation of the anti-RIBEYE B-domain antibody with RIBEYE B-domain antigen blocked immunodetection of RIBEYE B-domain. **d** Confocal image of RIBEYE B-domain immunoreactivity in the OPL showing the characteristic horseshoe shape of cone and rod photoreceptor ribbons

retinal sections was restricted to rod bipolar cells (see below) consistent with previous observations (e.g., Specht et al. 2007).

Mouse monoclonal anti-PKCα antibody (0.1 mg/ml; GE Healthcare UK, Buckinghamshire, England) was raised against amino acids 312–323 of bovine PKCα. According to the manufacturer, this antibody stains a single band (79 kDa) on Western blots, which corresponds to the α isoform of PKC (Kosaka et al. 1998).

The following secondary antibodies were used for immunofluorescence measurements: Alexafluor 594 goat anti-rabbit antibody (A-11012), Alexafluor 594 goat anti-mouse antibody (A-11005), Alexafluor 488 goat anti-rabbit antibody (A-11008), and Alexafluor 488 goat anti-mouse antibody (A-11001; Molecular Probes, Eugene, Ore., USA).

Western blot analysis

Mice were deeply anesthetized with sodium pentobarbital (45 mg/kg, i.p.). Brains and retinas were quickly removed and immersed in liquid nitrogen and stored at −70°C. The tissues were homogenized for 5 min on ice in twice the original volume of ice-cold homogenization buffer consisting of 20 mM TRIS, pH 7.4, 7 M urea, 1 mM dithiothreitol (DTT), 1 mM phenylmethylsulfonyl fluoride, and 10% protease inhibitor cocktail (Sigma-Aldrich). Cellular debris and nuclei were removed by centrifugation (800*g*) for 10 min. The supernatants were diluted with sample buffer consisting of 300 mM TRIS, 10% sodium dodecyl sulfate (SDS), 25% glycerol, 0.03% bromophenol blue, and 10 mM DTT. Total protein (25 μg/lane) was separated on 5%–20% gradient SDS–polyacrylamide gels (ATTO, Tokyo, Japan) and transferred onto polyvinylidene fluoride membranes (ATTO). The membranes, blocked with 5% skim-milk in phosphate buffer saline (PBS; 0.1 M) containing 0.1% Tween-20 (TPBS), were incubated with primary antibody overnight at 4°C and then with secondary antibody at room temperature for 1 h. Immunoreactivity was visualized by using the enhanced chemiluminescent (ECL) detection kit (GE Healthcare, UK) with LAS100 (Fuji-Film, Tokyo, Japan). Kaleidoscope Prestained Standard (Bio-Rad Japan, Tokyo, Japan) was used as a protein-size marker.

Immunocytochemistry

Dissociated mouse bipolar cells were obtained as follows for all experiments. Mice were deeply anesthetized with sodium pentobarbital (45 mg/kg, i.p.), and sections of retina were excised and incubated for 30 min in a mixture of papain (1.2 U/retina, Sigma-Aldrich), hyaluronidase (2.25 mg/retina, Sigma-Aldrich), and collagenase (2.25 mg/retina, Sigma-Aldrich) in Ames' medium (30 ml, Sigma-Aldrich) and then for another 30 min in papain (1.2 U/retina, Sigma-Aldrich) in Ames' medium. Specimens were then treated with protease inhibitor (10% L8531; Sigma-Aldrich) followed by DNase (3%; Sigma-Aldrich) in Ames' medium and mechanically triturated by using a pipette. A drop of cell suspension was spread underneath a coverslip within the 100-μm-wide space between it and the glass slide. The cell suspensions were imaged with a confocal laser scanning microscope (LSM510-16; Carl Zeiss, Oberkochen, Germany). Scanning was performed (512×512 pixels) with Plan-Achromat 63×/1.4 Oil differential interference contrast (DIC) or Plan-Neofluar 100×/1.3 Oil DIC by using the same parameters for cells from both wild-type and mGluR6-deficient mice. To account for fluorescent variability between cells, the intensity of fluorescence from the dendritic tip was divided by that from the axon terminal for each dissociated cell. The fluorescent intensity at the cell bodies and axons for all cells was first equilibrated by adjusting the brightness and contrast with Adobe Photoshop 7.0 (San Jose, USA). Thus, normalized fluorescent intensities were compared at the dendrites of both groups.

Retinal sections for immunoelectron and light microscopy studies were obtained as follows. Mice were deeply anesthetized with sodium pentobarbital (45 mg/kg, i.p.) and then perfused with a mixture of 4% paraformaldehyde and 0.01% glutaraldehyde in cacodylate buffer, pH 7.4. Retinas were excised and immersed in the same fixative for 20 min, irradiated with microwaves for 10 min, and rinsed with and cryoprotected in 30% sucrose-0.1 M phosphate buffer (pH 7.4). For light microscopy, retinas were fixed with 4% paraformaldehyde in cacodylate buffer, pH 7.4, for 3 h. Cryosections were then processed for conventional fluorescence microscopy and pre-embedding immunoelectron labeling as previously described (Sawada and Esaki 2002). For staining for electron microscopy, the diaminobenzidine (DAB) product was intensified by silver and substituted with gold after the ABC reaction as previously described (Sassoè-Pognetto et al. 1994).

Morphological characterization

The mGluR6-deficient and wild-type mice were maintained on a 12-h light/dark cycle for 1 week. The mice were deeply anesthetized with sodium pentobarbital (45 mg/kg, i.p.) 2 h before lights-off for light-adaptation experiments and 2 h before lights-on for dark adaptation experiments. To obtain enhanced-light-adapted retinas, mice were exposed to a tungsten lamp (about 2000 lux) directly facing them for 2 h in addition to room light (about 500 lux). This level of illumination was bright enough to exceed the rod dynamic range but remained within the dynamic range of photopic (pure-cone) vision so that rhodopsin pigments were not

exhaustively bleached. Preparation of light-adapted retinas was carried out under room light, and that of dark-adapted retinas was undertaken under infra-red converter optics (Noctovision, NEC, Tokyo, Japan). For all adaptation conditions, the animals were perfused with a mixture of 4% paraformaldehyde and 0.01% glutaraldehyde in phosphate buffer, pH 7.4. The posterior halves of the eyeballs were excised and processed separately for light and electron microscopy.

The roundness of rod bipolar invaginating dendrite cross-sectional contours was measured by using NIH Image J (National Institutes of Health, Bethesda, MD, USA) where circularity is defined as $4\pi * \text{area}/\text{square}(\text{perimeter})$; increasingly rounded shapes are indicated by circularity values approaching 1.0. Cross-sectional contours of dendrites from electron micrographic prints at ×15,000 magnification were obtained on transparent sheets and scanned for digital processing by using NIH Image J. The same procedure was also used to measure dendrite volumes. Twenty samples were collected from three mice (n=60 samples/data point).

To assess the roundness of the axon terminal contours, we measured the axonal radial standard deviation and compared the values obtained to those reported for goldfish bipolar cells by Job and Lagnado (1998). The radial standard deviation is the standard deviation from the center of an area to its outer boundary, calculated as a percentage of the mean radial distance; increasingly rounded shapes are indicated by radial standard deviation values approaching 0. Images used to calculate radial standard deviation were taken from confocal images (×63 objective, z-axis step size, 0.6 μm; LSM510-16, Carl Zeiss) of radial sections obtained by using a cryostat (Sakura Finetek, Tokyo, Japan) and immunostained with anti-PKCα antibody. Three radial sections from various locations in each mouse retina were imaged, and the radial standard deviation was calculated for ten neighboring rod bipolar axon terminals from each section (n=30 terminals/mouse). Relatively large terminal swellings of rod bipolar axon terminals (major axis: ≥5 μm; minor axis: ≥3 μm) were used for radial standard deviation measurements. To calculate radial standard deviation values by using NIH Image J, the contour of each PKCα-labeled rod bipolar axon terminal was traced, and 16 radial lines were drawn from the center of the terminal to the outer axon boundary; 90 radial standard deviation values were obtained for three mice from each of the four experimental groups (light-adapted wild-type; light-adapted mGluR6-deficient; dark-adapted wild-type; dark-adapted mGluR6-deficient).

Data analysis

The data in the text and figures are presented as the means±SEM. The significant differences between groups were assessed by an unpaired two-tailed Student's t-test or one-way analysis of variance (ANOVA) followed by the Turkey-Kramer's post hoc multiple comparison test. Null hypotheses were rejected at the 0.05 level.

Results

Ectopic ribbons in mGluR6-deficient rod and ON-cone bipolar dendrites

Electron-dense structures resembling axonal synaptic ribbons were frequently observed in the invaginating dendrites of rod and ON-cone bipolar cells in mGluR6-deficient mouse retinas but not wild-type mouse retinas (Tsukamoto et al. 1999). During the course of this study, we used serial-section analysis to distinguish between the pre- and postsynaptic processes because, in single sections, the presynaptic processes emanating from the photoreceptor terminal and intermingling with the postsynaptic dendrites might have appeared to be postsynaptic dendrites (Brandon and Lam 1983; Linberg and Fisher 1988). We thus verified that the dendritic profiles that contained these electron-dense structures were not contained in the presynaptic extensions from the photoreceptor terminal. The electron-dense structures in the postsynaptic dendrites showed some degree of polymorphism (Fig. 2a–e), unlike the regularly shaped bilaminated synaptic ribbons observed at the axon terminals of bipolar or photoreceptor cells. As a result of this difference in their lamination and shape, we initially distinguished ribbon-like structures from ectopic ribbons. Although the cross-section of the ribbon-like structures varied in shape, viz., circular (Fig. 2c), rectangular (Fig. 2d), and semicircular (Fig. 2e), the straight or curved plates comprising them had the same thickness and electron-density as the bilaminated ribbons (Fig. 2a, b). In addition, the ribbon-like structures showed the same anti-RIBEYE immunoreactivity as synaptic ribbons (Fig. 3g–l). Therefore, because of the similarity of the two structures, we refer herein to both bilaminated ribbons and non-laminated ribbon-like structures in bipolar cell dendrites as ectopic ribbons. No synaptic density was seen at the dendrite cell membranes in close apposition to ectopic ribbons. The ectopic ribbons were freely floating in the cytoplasm and also frequently surrounded by a halo of vesicles that resembled presynaptic vesicles in shape and size (Fig. 2a–c).

Because the α subunit of a heterotrimeric G-protein ($G\alpha_o$) is known to mediate the mGluR6 signal and membrane potential of retinal ON-bipolar cells (Dhingra et al. 2000, 2002), we examined the retinas of $G\alpha_o$-deficient mice for the presence of ectopic ribbons. Indeed, ectopic ribbons were observed in the invaginating dendrites of rod bipolar cells in $G\alpha_o$-deficient mice (Fig. 2f, g).

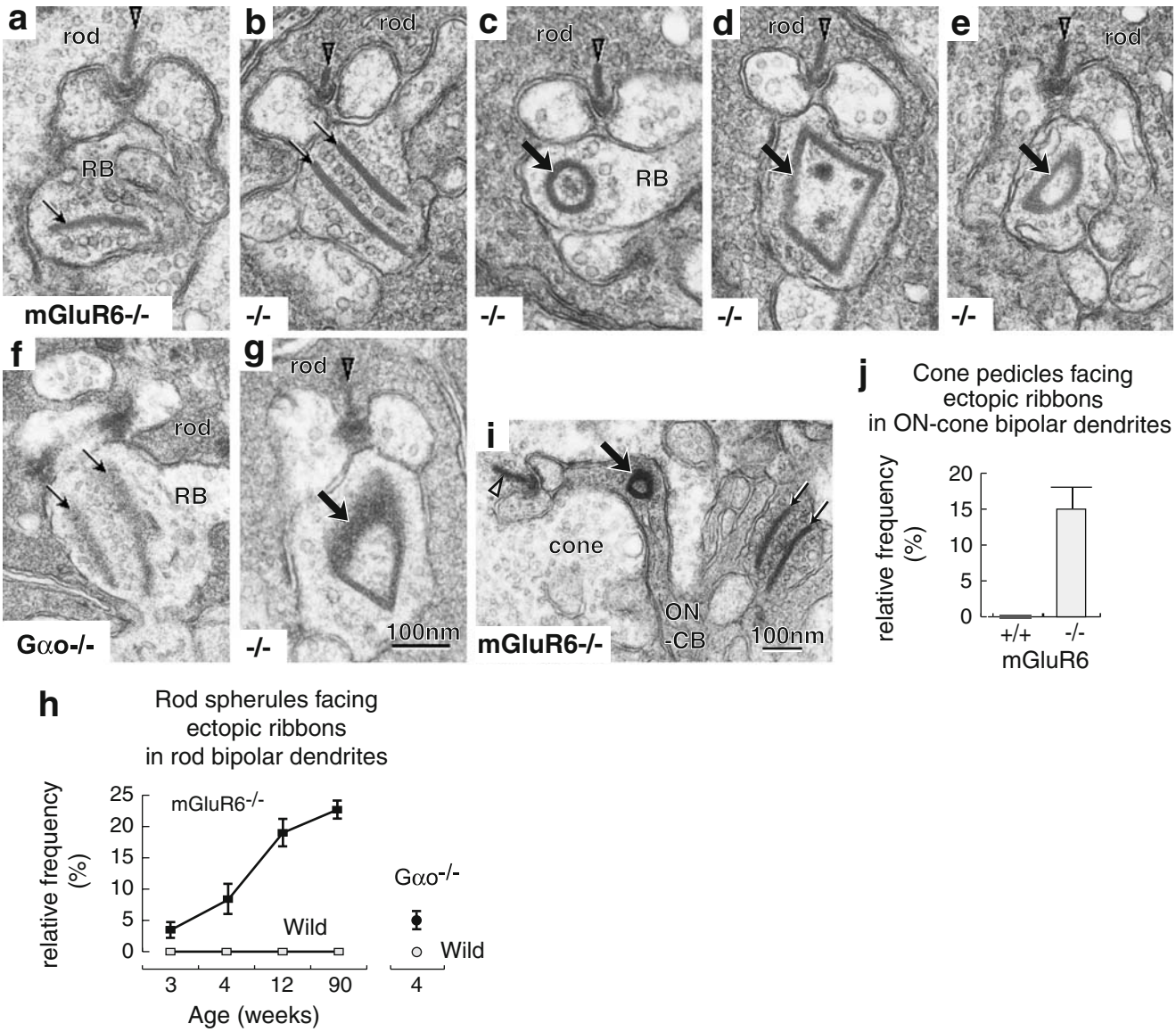

Fig. 2 Morphology and occurrence frequency of ectopic ribbons in rod and ON-cone bipolar cells. **a**–**g**, **i** Electron micrographs of ectopic ribbons (*thin arrows*) and ribbon-like structures (*thick arrows*) in rod (*RB*) and ON-cone bipolar (*ON-CB*) cell invaginating dendrites found opposite normal synaptic ribbons (*arrowheads*). The ectopic ribbons form lines (**a**) or parallel lines (**b**, **f**, **i**). The ribbon-like structures are circular (**c**, **i**), rectangular (**d**), or semi-circular (**e**, **g**). **a**–**e**, **i** mGluR6-deficient mice (−/−). **f**, **g** $G\alpha_o$-deficient mice (−/−). **h** Effect of age on the percentage of rod spherules facing ectopic ribbons in rod bipolar invaginating dendrites. Data were collected at 3, 4, 12, and 90 weeks for wild-type (*open rectangles*) and mGluR6-deficient (*closed rectangles*) mice, and at 4 weeks for wild-type (*open circle*) and $G\alpha_o$-deficient (*closed circle*) mice. **j** Percentage of cone pedicles facing ectopic ribbons in ON-cone bipolar cell invaginating dendrites in mGluR6-deficient and wild-type mice (age: 12 weeks)

As expected, normal presynaptic ribbons were observed in the rod bipolar axonal terminals of wild-type and of mGluR6- and $G\alpha_o$-deficient mice (data not shown). The normal ribbons lay at right angles to the presynaptic membrane, forming synapses with a dyad of postsynaptic processes. In contrast, in mGluR6-deficient and $G\alpha_o$-deficient mouse retinas, the invaginating dendritic tips of the rod bipolar cells were enlarged and round (Fig. 2a–g; see also below), unlike the elongated parallel dendrites found in wild-type rod bipolar cells (see also below).

To determine when ectopic ribbons appear in the OPL, we determined the number of ribbons in wild-type and mGluR6-deficient mice at several time points (n=3 per age group, Fig. 2h). During retinal postnatal development in mice, the dendrites of bipolar cells invaginate the photoreceptor terminals at 2 weeks (Blanks et al. 1974). The number of ribbon synapses in the inner plexiform layer (IPL) plateaus at 3 weeks (Fisher 1979). In rats, mGluR6 receptor density and synaptic formation in the OPL reaches adult levels at 4 weeks (Nomura et al. 1994). We

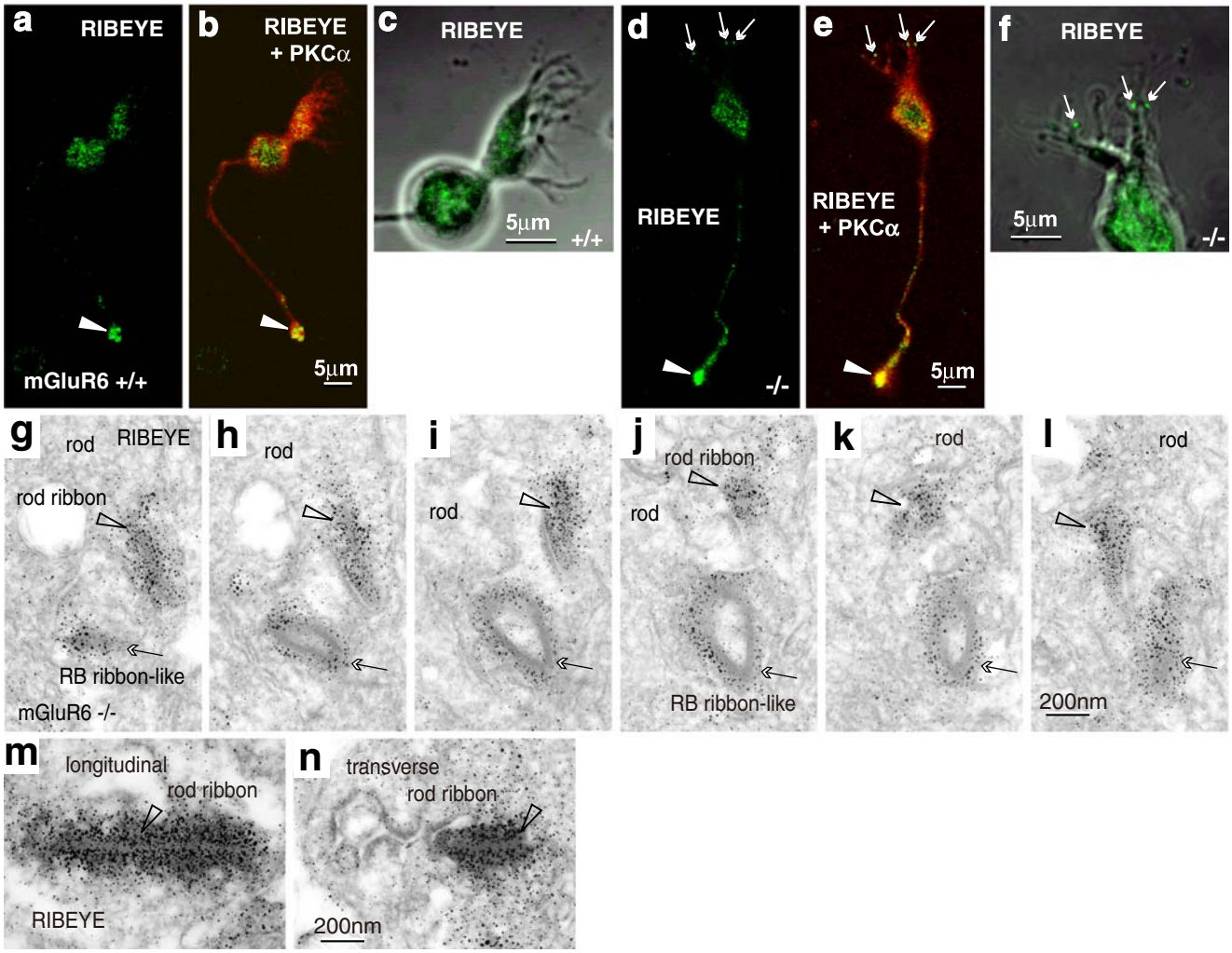

Fig. 3 Immunocytochemistry of rod bipolar cells with anti-RIBEYE B domain (ribbon-specific protein) antibody. **a**–**f** Confocal immunofluorescent images of dissociated rod bipolar cells. Whole cells are double-labeled for RIBEYE (*green*) and protein kinase Cα (*PKCα*, *red*), where PKCα is specific for rod bipolar cells (**b**, **e**). RIBEYE is expressed at the axon terminal (*arrowhead*) and soma in the wild-type (+/+) retina (**a**, **b**), but at the dendritic tips (*arrows*), axon terminal (*arrowhead*) and soma in the mGluR6-deficient (−/−) retina (**d**, **e**). Three loci of RIBEYE immunoreactivity (*arrows*) are clearly observed in mGluR6-deficient (−/−) rod bipolar cell dendrites (**f**), but not in wild-type (+/+) rod bipolar cell dendrites (**c**), where their fine dendritic processes (**c**, **f**) can be identified under differential interference contrast (*gray*). **g**-**n** Electron micrographs of mGluR6-deficient (−/−) mouse retina immunolabeled for RIBEYE. Six consecutive sections (**g**–**l**) showed an immunopositive ribbon-like structure (*arrows*) in the invaginating dendrite of a rod bipolar cell (*RB*) and an immunopositive normal ribbon (*arrowheads*) in the rod photoreceptor spherule. The shape of the rod ribbon sectioned obliquely in **g**–**l** (*arrowheads*) is obscured but forms a distinct immunopositive pair of bars when sectioned perpendicularly to the ribbon plate (**m**, longitudinal ribbon axis; **n**, transverse ribbon axis)

determined the percentage of rod photoreceptor spherules associated with ectopic ribbons in invaginating rod bipolar dendrites at 3 and 4 weeks (n=~200 rods/mouse; n=3 per age group), and at 12 and 90 weeks (n=~100 rods/mouse; n=3 per age group). The percentage in wild-type mice was zero at all ages examined. In contrast, the percentage in mGluR6-deficient mouse retina increased from 3.5%±1.1% at 3 weeks to 8.4%±2.4% at 4 weeks and then doubled to a plateau level of about 19%±2.1% at 12 weeks and 22.7%±1.3% at 90 weeks (Fig. 2h). Each rod spherule had two invaginating bipolar dendrites. Hence, approximately 10% of the invaginating processes had ectopic ribbons. As each rod bipolar cell had about 15–20 fine invaginating dendrites, one to two invaginating processes of each rod bipolar cell had ectopic ribbons.

The percentage of rod photoreceptor spherules associated with ectopic ribbons in invaginating rod bipolar dendrites was also determined in $G\alpha_o$-deficient mice. The expression of $G\alpha_o$ is more widespread than mGluR6, which is expressed exclusively in retinal ON-bipolar cells. As a result, $G\alpha_o$-deficient mice do not survive much longer than 4 weeks. Therefore, the percentage in $G\alpha_o$-deficient mice

was determined only at 4 weeks; 4.7%±0.9% of rod photoreceptor spherules were associated with ectopic ribbons in invaginating rod bipolar dendrites. This result was close to that observed at 4 weeks (unpaired *t*-test, two-tailed P=0.21, n=3 mice/group) in mGluR6-deficient mice. Thus, mGluR6 and $G\alpha_o$ deficiency showed a similar effect on the distribution of ectopic ribbons.

Cone pedicles associated with ON-cone bipolar cell dendrites were examined at the age of 12 weeks. ON-cone bipolar dendrites made invaginating contacts with concave ribbon-associated pedicle membranes. As in rod bipolar cells, ON-cone bipolar cell dendrites expressed mGluR6 (Ueda et al. 1997; Vardi and Morigiwa 1997). As observed in rod bipolar cells from mGluR6-deficient mice (Fig. 2a–e), ectopic ribbons were frequently located in the invaginating dendrites of mGluR6-deficient ON-cone bipolar cells (Fig. 2i). In contrast, in wild-type mice at the same age, no ectopic ribbons were observed in the invaginating dendrites of ON-cone bipolar cells. The percentage of cone pedicles with ectopic ribbons was zero in wild-type mice (n=~50 cones/mouse; n=3 mice) but was 15.4%±3.1% (n=50 cones/mouse; n=3 mice) in mGluR6-deficient mice (Fig. 2j). Thus, ectopic ribbons were observed in both rod and ON-cone bipolar cells of mGluR6-deficient mouse retinas, but not in wild-type mice.

RIBEYE and synaptophysin distribution

Ectopic ribbons and their associated vesicles were characterized by immunohistochemistry of the ribbon-specific protein RIBEYE (Fig. 3) and synaptic-vesicle-specific protein synaptophysin (Fig. 4), respectively. Anti-RIBEYE B-domain and anti-synaptophysin antibodies were applied to dissociated rod bipolar cells from both wild-type and mGluR6-deficient mice for confocal immunofluorescence microscopy and to retinal sections for immunoelectron microscopy.

As expected, in dissociated cells from wild-type mice (n=28 cells), the axon terminals of PKCα-immunopositive rod bipolars were strongly immunoreactive for RIBEYE (Fig. 3a, b). The somata of these same cells were weakly immunoreactive for RIBEYE, whereas the fine dendritic processes were not immunoreactive for RIBEYE (Fig. 3c). In contrast, in dissociated cells from mGluR6-deficient mice (Fig. 3d–f), the fine dendritic processes and the axon terminals were strongly immunoreactive for RIBEYE. Similar to the wild-type cells, the somata of mGluR6-deficient cells was weakly immunoreactive for RIBEYE. As the anti-RIBEYE B-domain antibody used here also reacts with the transcription factor CtBP2, the immunoreactivity of the somata might also be attributable to this transcription factor, which is contained in the nucleus (Schmitz et al. 2000).

Punctate RIBEYE immunoreactivity was seen at two to three loci on the dendritic arbors of mGluR6-deficient rod bipolar cells (n=130 loci from 51 cells; Fig. 3f). Rod bipolar cells have 15–20 fine invaginating dendrites. Therefore, about 10%–20% of invaginating dendrites were immunopositive for RIBEYE. This is consistent with the percentage of cone pedicles associated with ectopic ribbons described here (Fig. 2h).

Consecutive sections of a rod spherule showed a normal ribbon in the rod spherule and an ectopic ribbon in the invaginating rod bipolar dendrite (Fig. 3g–l). The structure of the normal ribbon in the rod spherule of these figures was obscured because the sections had been cut obliquely. Therefore, conventionally shaped, RIBEYE-immunopositive normal ribbons were examined (Fig. 3m, n) in which the sections were perpendicular to the ribbon plates (**m**: longitudinal axis of a ribbon; **n**: transverse axis of a ribbon). The consecutive sections of the rod-rod bipolar junction (Fig. 3g–l) also showed the three-dimensional shape of a non-laminated electron-dense structure in the rod bipolar dendrite. This structure was composed of two RIBEYE-immunopositive curved plates that formed a bivalve shape with an expanded inner space devoid of RIBEYE immunoreactivity. This result suggested that the non-laminated electron-dense structures in bipolar dendrites (Fig. 2c, d, e, g, i) contained ribbon protein.

The distribution of the synaptic-vesicle marker synaptophysin in dissociated rod bipolar cells and retinal cryosections was examined by confocal immunofluorescence microscopy (Fig. 4a–f). The axon terminal of rod bipolar cells was strongly immunoreactive in both wild-type (Fig. 4a, b) and mGluR6-deficient mice (Fig. 4d, e). The axonal processes and the cytoplasm surrounding the nuclei were weakly immunoreactive for synaptophysin, whereas the fine dendrites were not immunoreactive for synaptophysin in either wild-type (n=13 cells) or mGluR6-deficient (n=13 cells) mice. In retinal sections (Fig. 4c, f) from both wild-type and mGluR6-deficient mice, no synaptophysin immunoreactivity was observed in the primary dendrites or somatic cytoplasm of rod bipolar cells. In contrast, intense synaptophysin immunolabeling was found in rod photoreceptor spherules in both wild-type (Fig. 4c) and mGluR6-deficient (Fig. 4f) retinas. Thus, the distribution of synaptophysin did not correlate with the distribution of ectopic ribbon proteins in the dendrites of mGluR6-deficient rod bipolar cells.

The images in electron micrographs of anti-synaptophysin-labeled synaptic junctions between rod photoreceptor spherules and rod bipolar dendrites (Fig. 4g, h) and rod bipolar axon terminals (Fig. 4i) were consistent with the results obtained for dissociated cells. In both wild-type and mGluR6-deficient mice, the presynaptic cytoplasm of rod spherules (Fig. 4g, h) and the cytoplasm around synaptic ribbons in rod bipolar axon terminals (Fig. 4i:

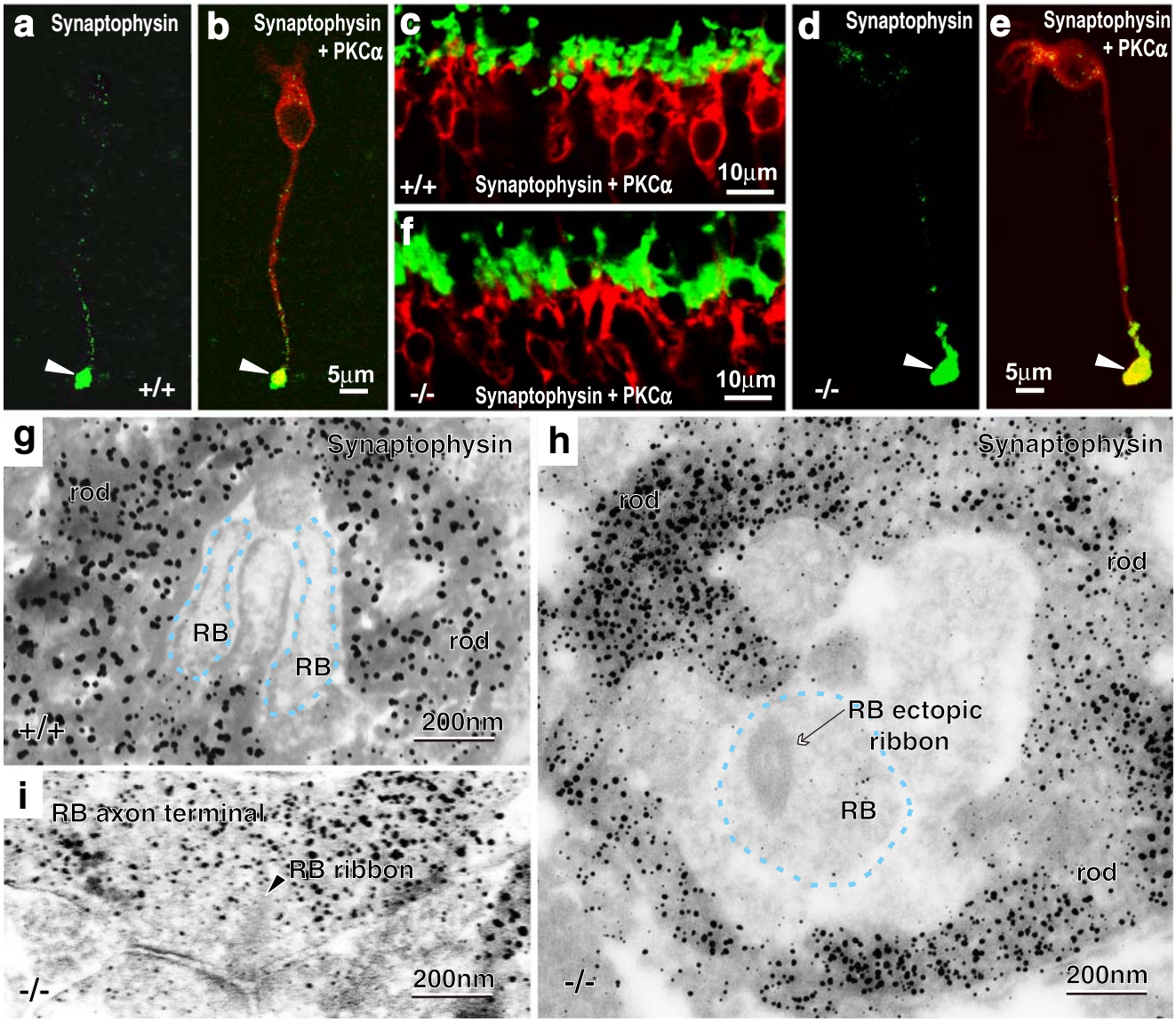

Fig. 4 Immunocytochemistry of rod bipolar cells by using anti-synaptophysin (synaptic-vesicle-specific protein) antibody. Confocal laser-scanning micrographs of dissociated cells (**a**, **b**, **d**, **e**) and retinal cryosections (**c**, **f**) double-labeled for synaptophysin (*green*) and PKCα (*red*). Synaptophysin immunoreactivity was prevalent at the axon terminal (*arrowheads*) but negligible at the dendrites of rod bipolar cells dissociated from both wild-type (**a**, **b** +/+) and mGluR6-deficient (**d**, **e** −/−) mice. In the OPL, synaptophysin immunoreactivity was evident across the rod photoreceptor spherules (*green*) but negligible in the primary dendrites of rod bipolar cells in both wild-type (**c** +/+) and mGluR6-deficient (**f** −/−) mice. **g-i** Electron micrographs of mouse retinas immunolabeled for synaptophysin. Immunoreactivity for synaptophysin was negative in the parallel invaginating dendrites of rod bipolar cells (*RB*, *dotted blue lines*) in the wild-type retina (**g**). In the mGluR6-deficient (−/−) retina (**h**), an ectopic ribbon (*arrow*) was present in the large round invaginating dendrite of an RB cell (*dotted blue line*) where synaptophysin immunoreactivity was negligible. In both wild-type (**g** +/+) and mGluR6-deficient (**h** −/−) retinas, synaptophysin immunoreactivity was found in the rod cytoplasm (*green* immunolabeled rod spherules in **c** [+/+] and **f** [−/−]). Synaptophysin immunoreactivity was also evident in the cytoplasm of RB axon terminals (**i** −/−) around the ribbon (*arrowhead*); RB axon terminal (green in **d** [−/−]) *arrowhead*)

mGluR6-deficient; wild-type data not shown) were immunopositive for synaptophysin. The postsynaptic invaginating dendrites of rod bipolar cells in wild-type mice were slit-like in shape, whereas in mGluR6-deficient mice, the dendrites were enlarged, round, and contained ectopic ribbons. Despite the difference in dendrite morphology, no synaptophysin immunoreactivity was observed in wild-type or mGluR6-deficient mice (Fig. 4g, h). The small dot-like labeling in mGluR6-deficient rod bipolar dendrites (Fig. 4h) was typical of noise associated with this immunolabeling method.

These results showed that the ectopic ribbons found in mGluR6-deficient rod bipolar dendrites contained RIBEYE protein, the major synaptic ribbon component. However,

vesicles adjacent to the ectopic ribbons did not contain synaptophysin protein, one of the constituent proteins of synaptic vesicles found at axon terminals.

Ectopic synaptic ribbons in OFF-cone bipolar dendrites

In this study, ectopic ribbons were observed not only in mGluR6-deficient rod and ON-cone bipolar dendrites, but also under the basal surface of cone photoreceptor pedicles in dendrites of OFF-cone bipolar cells (Dowling 1987) in both wild-type (Fig. 5a) and mGluR6-deficient (Fig. 5b) mice. Ectopic ribbons in OFF-cone bipolar cell dendrites have been observed in several mammalian species (Kolb 1977; Spiwoks-Becker et al. 2000) but have not yet been fully characterized. Like those reported by Spiwoks-Becker et al. (2000), the ectopic ribbons in dendrites of OFF-cone bipolar cells were not directed at any synaptic density on the cell membrane and floated in the cytoplasm. The overall frequency of ectopic ribbons in OFF-cone bipolar cell dendrites was determined for both wild-type and mGluR6-deficient mice. The frequency was evaluated as the percentage of cone photoreceptor pedicles associated with ectopic ribbons in OFF-cone bipolar dendrites (Fig. 5c). The frequency of ectopic ribbons in OFF-cone bipolar cell dendrites of wild-type and mGluR6-deficient mice was not significantly different (mean ± SEM; 14.9%±1.2%, wild-type; 12.7%±2.4%, mGluR6-deficient mice; n=50 cones/mouse; unpaired t-test, two-tailed P=0.48, n=3 mice/group). On average, there was one ectopic ribbon for every seven cone pedicles.

The depth and ramification of the axon terminals in the IPL of the reconstructed whole cells were used to classify bipolar cells into one of ten types as previously described (Ghosh et al. 2004; Ivanova et al. 2006). Interestingly, ectopic ribbons were found only in T2 OFF-cone bipolar cells (Fig. 5d, h; 5±1.9 ribbons; n=3 cells). T2 cells were similar to type 2 bipolar cells described by Ivanova et al. (2006), of which types 1–4 were OFF-cone bipolars that ramified their axon terminals in the outer half of the IPL. Notably, T2 cells had the largest number of presynaptic ribbons at the axon terminals (T2: 162±4.2 ribbons; n=3 cells) among the four OFF-bipolar cell types. Furthermore, ectopic ribbons were not observed in the dendrites of T1, T3, and T4 cells, which all had significantly fewer presynaptic ribbons at the axon terminals than did T2 cells (T1: 92±9.0 ribbons, $^{**}P$=0.003; T3: 56±3.5 ribbons, $^{**}P$<0.0001; T4: 64±6.7 ribbons, $^{**}P$<0.0001; one-way ANOVA followed by Tukey-Kramer's test, n=3 mice/group; Fig. 5i). T2 cells also had axonal cylinders that were approximately twice as thick (T2: 1.26±0.12 μm: measured 5 μm below the soma) than the other cell types (T1: 0.60±0.05 μm, $^{**}P$=0.0015; T3: 0.64±0.01 μm, $^{**}P$=0.0014; T4:0.61±0.06 μm, $^{**}P$=0.0021; one-way ANOVA followed by Tukey-Kramer's test, n=3 mice/group; Fig. 5e–g, j).

Fig. 5 Detection of ectopic ribbons and identification of OFF-cone bipolar cell types (T1–T4). **a**, **b** Ectopic ribbons (*arrows*) were found in OFF-cone bipolar dendrites (*OFF-CB*) of both wild-type (**a** +/+) and mGluR6-deficient (**b** −/−) mice. **c** Percentage (mean ± SEM) of cone pedicles facing ectopic ribbons in OFF-cone bipolar dendrites. Ectopic ribbons are present in OFF-cone bipolar cell dendrites in both wild-type (+/+) and mGluR6-deficent (−/−) mice (age: 12 weeks, n=3 mice/group). **d** Reconstruction of type T1–T4 OFF-cone bipolar cells from serial electron micrographs. OFF-bipolar cells were classified by the depth and ramification of their axon terminals in the inner plexiform layer (*IPL*). The depths of the axon terminal in the IPL for each type are as follows: T1: 28%, T2: 31%, T3: 38%, T4: 45% (*OPL* outer plexiform layer, *INL* inner nuclear layer). **e-g** Electron micrographs of the proximal portion of T1, T2, T3, and T4 OFF-cone bipolar cells. Axons in T2 cells are thicker and paler than those of T1, T3, and T4 axons. **h** Number of ectopic ribbons per cell in OFF-cone bipolar cell dendrites. Ectopic ribbons were found only in T2 cells (5±2, n=3 cells). Ectopic ribbons were not observed in T1, T3, or T4 cells. **i** Number of presynaptic ribbon synapses per cell at OFF-cone bipolar cell axon terminals. The number of ribbon synapses in T2 cells was significantly greater than in T1, T3, or T4 cells. **j** Diameter of axons 5 μm from the soma in OFF-cone bipolar cells. The axon diameter of T2 cells was significantly larger than in T1, T3, and T4 cells. **i**, **j** $^{**}P$<0.005 compared with the three other groups in each graph, Tukey-Kramer's test, n=3 mice/group

Morphology of rod bipolar invaginating dendrites and axon terminals

As noted earlier, the ultrastructure of rod bipolar dendrites that invaginated rod photoreceptor spherules were significantly different between wild-type and mGluR6-deficient mice (Fig. 2). This difference in morphology is potentially important, because the structure-function correlation has been well exemplified in the invaginating dendrites of fish horizontal cells; the formation of spinules depends on light adaptation in association with synaptic activity (Wagner and Djamgoz 1993; Behrens et al. 2000; Wagner and Kröger 2005). Although the same kind of correlation could not be expected, an investigation of the change in shape with special reference to ectopic ribbons was considered worthwhile. Therefore, we further analyzed the structural differences of rod bipolar invaginating dendrites and the factors involved in the structural changes (Fig. 6a–f). In cross sections of rod spherules, the invaginating dendrites of wild-type rod bipolar cells were small and elliptical or slit-like (Fig. 6a), whereas those of mGluR6-deficient rod bipolar cells were large and round (Fig. 6c). In three-dimensional reconstructions, wild-type dendrites resembled a pair of deflated balloons (Fig. 6b). In contrast, mGluR6-deficient dendrites resembled a pair of inflated balloons (Fig. 6d) and were frequently irregularly shaped and asymmetrical. However, the connections between the presynaptic ribbon and the post-synaptic triad of one bipolar

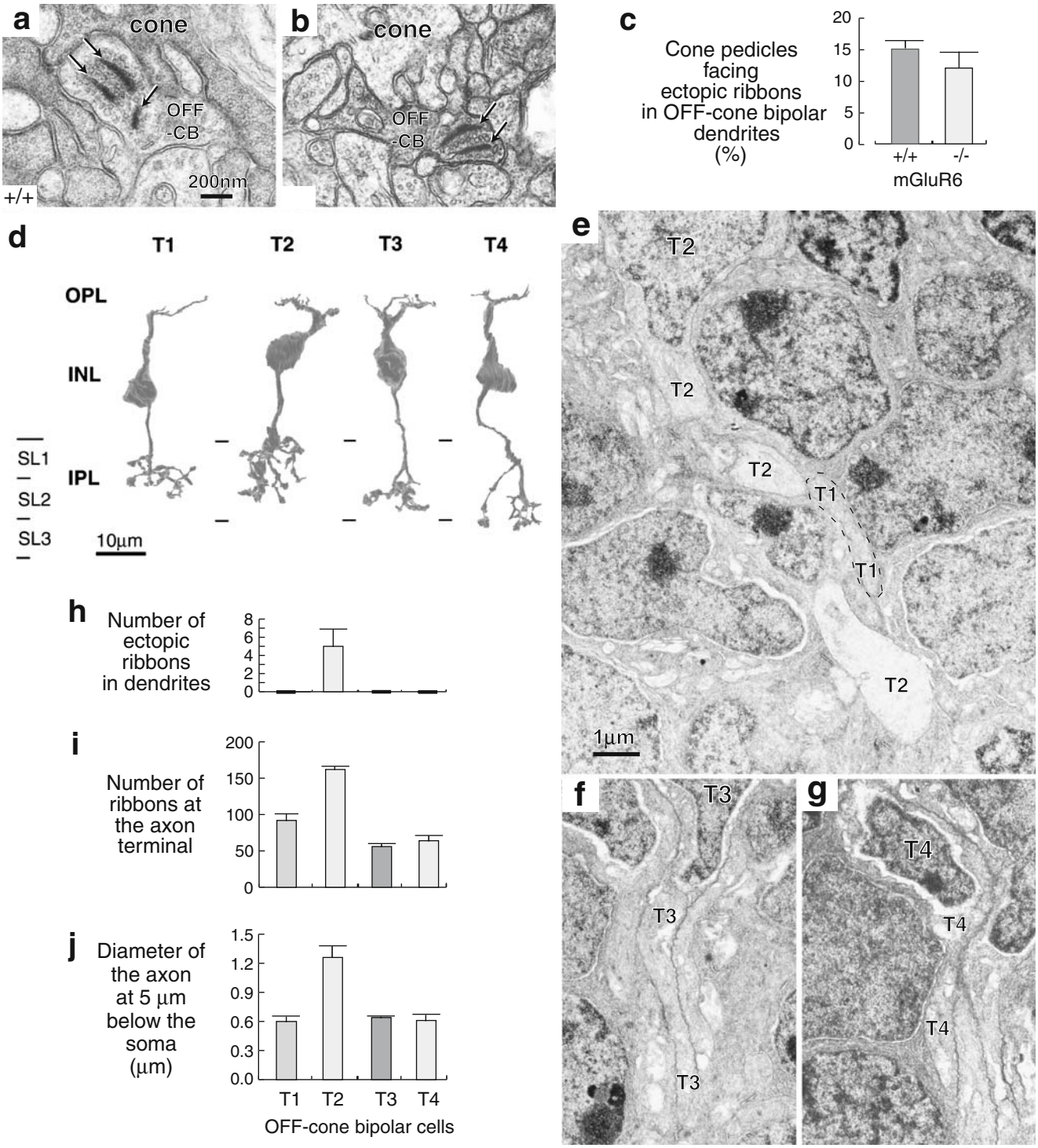

and two horizontal processes were invariably intact. Only the invaginating dendrites of the rod bipolar cells were morphologically different in mGluR6-deficient mice.

The extent of the morphological differences between invaginating dendrites in wild-type and mGluR6-deficient rod bipolar cells was evaluated by a statistical analysis of dendrite volume and shape by using serial sections from wild-type cells, mGluR6-deficient cells with ectopic ribbons, and mGluR6-deficient cells without ectopic ribbons (Fig. 6e, f). Cells were taken from 4- and 90-week-old mice.

At both 4 and 90 weeks, the volume of invaginating dendrites in mGluR6-deficient mice without ectopic ribbons (0.042±0.007 μm^3, 4 weeks; 0.074±0.007 μm^3, 90 weeks) was statistically greater than that of invaginating dendrites in

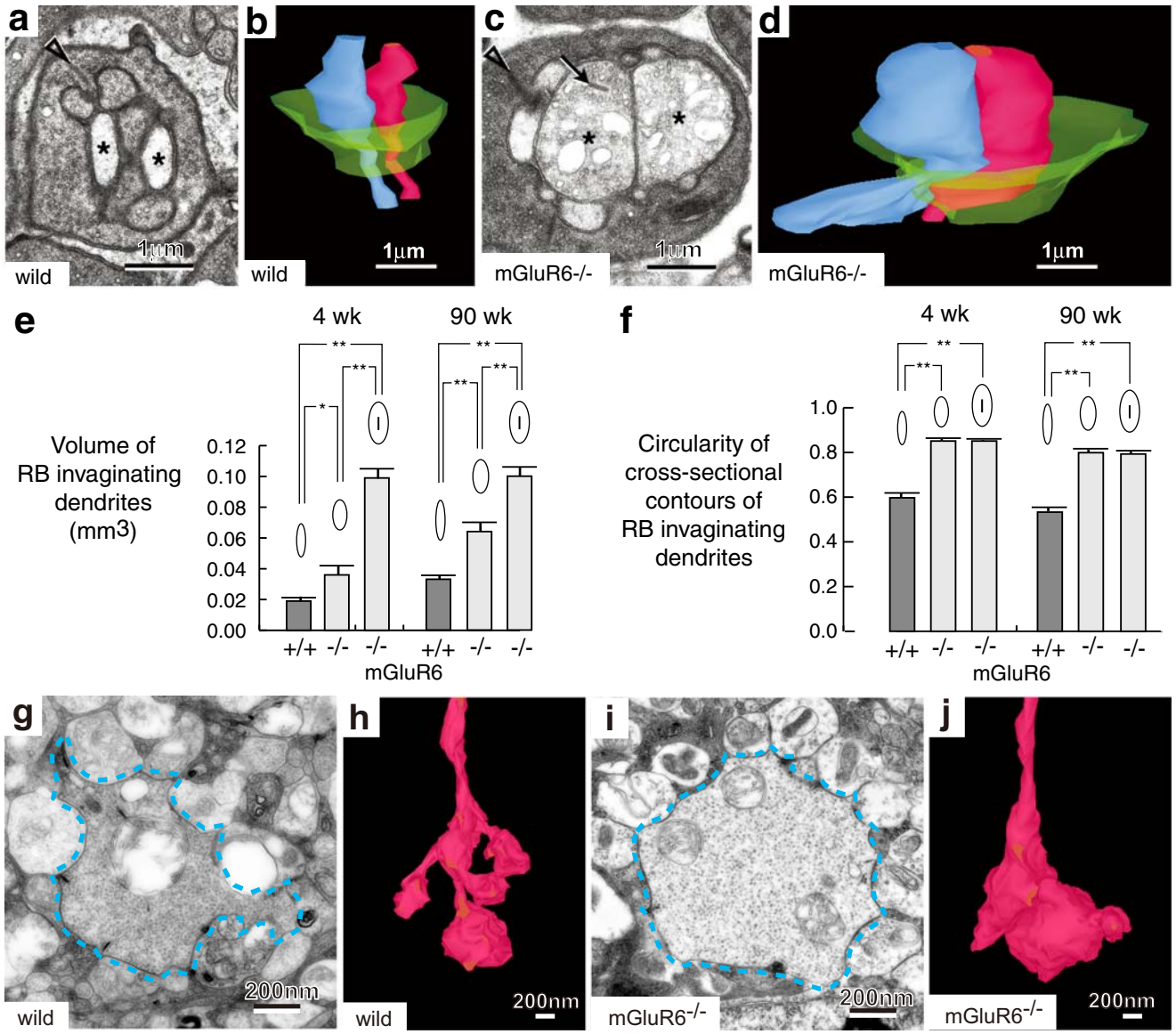

Fig. 6 Morphological differences between the invaginating dendrites and axon terminals of wild-type and mGluR6-deficient rod bipolar cells. **a**, **c** Electron micrographs of a pair of rod bipolar dendrites (*stars*) invaginating a rod photoreceptor terminal (cross sectional view). Normal synaptic ribbons (*arrowheads*) were observed in rod photoreceptor cytoplasm in both wild-type (**a**) and mGluR6-deficient (**c**) mice. An ectopic ribbon (*arrow*) was found only in rod bipolar dendrites of mGluR6-deficient mice (**c**). **b**, **d** Three-dimensional reconstructions of the dendritic processes (*blue*, *red*) resembled a pair of deflated balloons (**b**) in the wild-type (*wild*) and a pair of inflated balloons (**d**) in mGluR6-deficient (−/−) mice (*green* basal surface of rod photoreceptor cell). **e**, **f** Volume and circularity of rod bipolar invaginating dendrites in wild-type (+/+) and mGluR6-deficient (−/−) mice (*wk* week). Two groups of mGluR6-deficient dendrites were observed, those with and those without ectopic ribbons (*lines within ellipses* presence of ectopic ribbons). **e** **P*<0.05, ***P*<0.005; Tukey-Kramer's test, *n*=60/group. **f** ***P*<0.0001; Tukey-Kramer's test, *n*=60/group. **g**, **i** Electron micrographs of single sections of rod bipolar axon terminals from wild-type (**g**) or mGluR6-deficient (**i**) mice. The contour profile (*dotted blue line*) is rounder and smoother in mGluR6-deficient (**i**) than wild-type (**g**) mice. Retinas from both mice were prepared under conventional room-lighting conditions. **h**, **j** Three-dimensional reconstruction of a rod bipolar axon terminal. The terminal has several small distinct lobules in the wild-type (**h**) mouse but a single enlarged round lobule enclosed with other small lobules in the mGluR6-deficient (**j**) mouse retina

wild-type mice (0.022±0.002 µm^3, **P*=0.031, 4 weeks; 0.039±0.002 µm^3, ***P*=0.0029, 90 weeks; one-way ANOVA followed by Tukey-Kramer's test, *n*=60 dendrites/group; Fig. 6e). Furthermore, the volume of invaginating dendrites in mGluR6-deficient mice with ectopic ribbons (0.117±0.007 µm^3, 4 weeks; 0.118±0.007 µm^3, 90 weeks) was statistically far greater than that of invaginating dendrites in wild-type mice and in mGluR6-deficient mice without ectopic ribbons (***P*<0.0001 for 4 weeks or 90 weeks in both types of mice; one-way ANOVA followed by Tukey-

Kramer's test, n=60 dendrites/group; Fig. 6e). Hence, the volume of dendrites invaginating rod bipolar cells depended on the presence/absence of mGluR6 and the presence/absence of ectopic ribbons.

The roundness of dendrites invaginating rod bipolar cells was also examined by assessing dendrite circularity (Fig. 6f). The mGluR6-deficient invaginating dendrites with (0.85±0.006, 4 weeks; 0.79±0.011, 90 weeks) and without (0.85±0.009, 4 weeks; 0.80±0.013, 90 weeks) ectopic ribbons were both significantly rounder than the wild-type invaginating dendrites (0.60±0.017, 4 weeks; 0.53±0.018, 90 weeks; $^{**}P<0.0001$; one-way ANOVA followed by Tukey-Kramer's test, n=60 dendrites/group). However, the presence/absence of ectopic ribbons in mGluR6-deficient dendrites had no significant effect on dendrite roundness at 4 or 90 weeks ($P>0.99$, one-way ANOVA followed by Tukey-Kramer's test, n=60 dendrites/group). Hence, the roundness of dendrites invaginating rod bipolar cells depended on the presence/absence of mGluR6 but not on the presence/absence of ectopic ribbons.

The morphology of the axon terminals of rod bipolar cells was also examined (Fig. 6g–j). The axon terminals consisted of several lobules that had bulbous ends that were swollen and smoother in mGluR6-deficient mice than in wild-type mice. Similar differences in the surface topology of axon terminals have been noted in dark- and light-adapted rat rod bipolar cells (Behrens et al. 1998) whose light-adapted axon terminals are rounder and smoother than dark-adapted axon terminals. The release of glutamate from rod photoreceptors is reduced when they are exposed to light. Thus, rod bipolar cells in a light-adapted wild-type retina exposed to intense illumination with virtually null glutamate release are probably in a similar state to an mGluR6-deficient rod bipolar cell that fails to hyperpolarize upon exposure to glutamate. We therefore carried out the following experiments to determine whether morphological changes occur in invaginating dendrites and axon terminals in wild-type rod bipolar cells and furthermore to examine whether ectopic ribbons occur in the invaginating dendrites.

Effects of light adaptation on morphology of invaginating dendrites and axon terminals of rod bipolar cells

Dark and light adaptation affect the morphology of synaptic terminals of mixed rod-cone bipolar cells in goldfish retinas (Yazulla and Studholme 1992; Behrens and Wagner 1996; Job and Lagnado 1998) and of rod bipolar cells in rat retinas (Behrens et al. 1998). Behrens et al. (1998) used "bright-light" (850–900 lux) and "dim-light" (0.5–1 lux) exposure for over 4 h in order to mimic natural daylight and night-time conditions but observed only modest shape differences in the axon terminals of rat rod bipolar cells. We therefore exposed wild-type retinas to an enhanced-light-adapted condition of 2 h of intense illumination (2000 lux) in addition to room light (500 lux) after a week of 12 h light/dark cycles. As controls, mGluR6-deficient retinas were exposed to the same enhanced-light- or dark-adapted conditions. Job and Lagnado (1998) assessed the difference of axon terminal shape of mixed rod-cone bipolar cells in dark-adapted (convoluted shape) and light-adapted states (round shape) and quantitatively assessed the difference in roundness by measuring the radial standard deviation. To assess the roundness of mouse rod bipolar axon terminals, we adopted the radial standard deviation measurements for both wild-type and mGluR6-deficient mice subjected to dark or enhanced-light adaptation.

Radial cryosections of both dark- and enhanced-light-adapted retinas were immunolabeled with PKCα. In dark-adapted wild-type retinas, the PKCα-labeled axon terminals of rod bipolar cells (Fig. 7a) showed elongated profiles with irregular convoluted contours. In some cases, the axon terminals had small thin projections (dotted area and inset). In contrast, in enhanced-light-adapted wild-type mouse retinas (Fig. 7b), the PKCα-labeled axon terminals of rod bipolar cells showed a smoother and rounder profile, which was still convoluted but with fewer irregularities. Notably, this degree of roundness of axon terminals in wild-type retinas was obtained only with enhanced-light adaptation. As expected, in mGluR6-deficient mice, the PKCα-labeled axon terminals of rod bipolar cells in both dark- and enhanced-light-adapted retinas were ovoid with moderately convoluted contours (Fig. 7c, d). The general morphology of the rod bipolar axon terminals in mGluR6-deficient retinas was similar to that observed for enhanced-light-adapted wild-type mouse retinas, regardless of the adaptation conditions (Fig. 7b–d).

Most PKCα-labeled rod bipolar axon terminals in all retinas had diameters greater than 5 μm, but some had diameters of 3 μm or less. Small diameter terminals (1–3 μm) thought to represent terminal bulbs branching out from the major terminal swellings were excluded. The radial standard deviation of major rod bipolar cell axon terminal swellings was determined from representative optical sections of retinas (Fig. 7e, f) from dark- and enhanced-light-adapted wild-type and mGluR6-deficient mice (n=30 terminals/mouse, n=3 mice/group, Fig. 7a–d). No significant differences were observed in the axon terminal radial standard deviation among enhanced-light-adapted wild-type mice (18.4%±0.7%), dark-adapted mGluR6-deficient mice (18.4%±0.7%), and enhanced-light-adapted mGluR6-deficient mice (16.8%±0.6%). In contrast, the axon terminal radial standard deviation of dark-adapted wild-type mice was significantly greater (30.2%±1.1%, $^{**}P<0.0001$, one-way ANOVA followed by Tukey-Kramer's test, n=90 terminals/group) than that

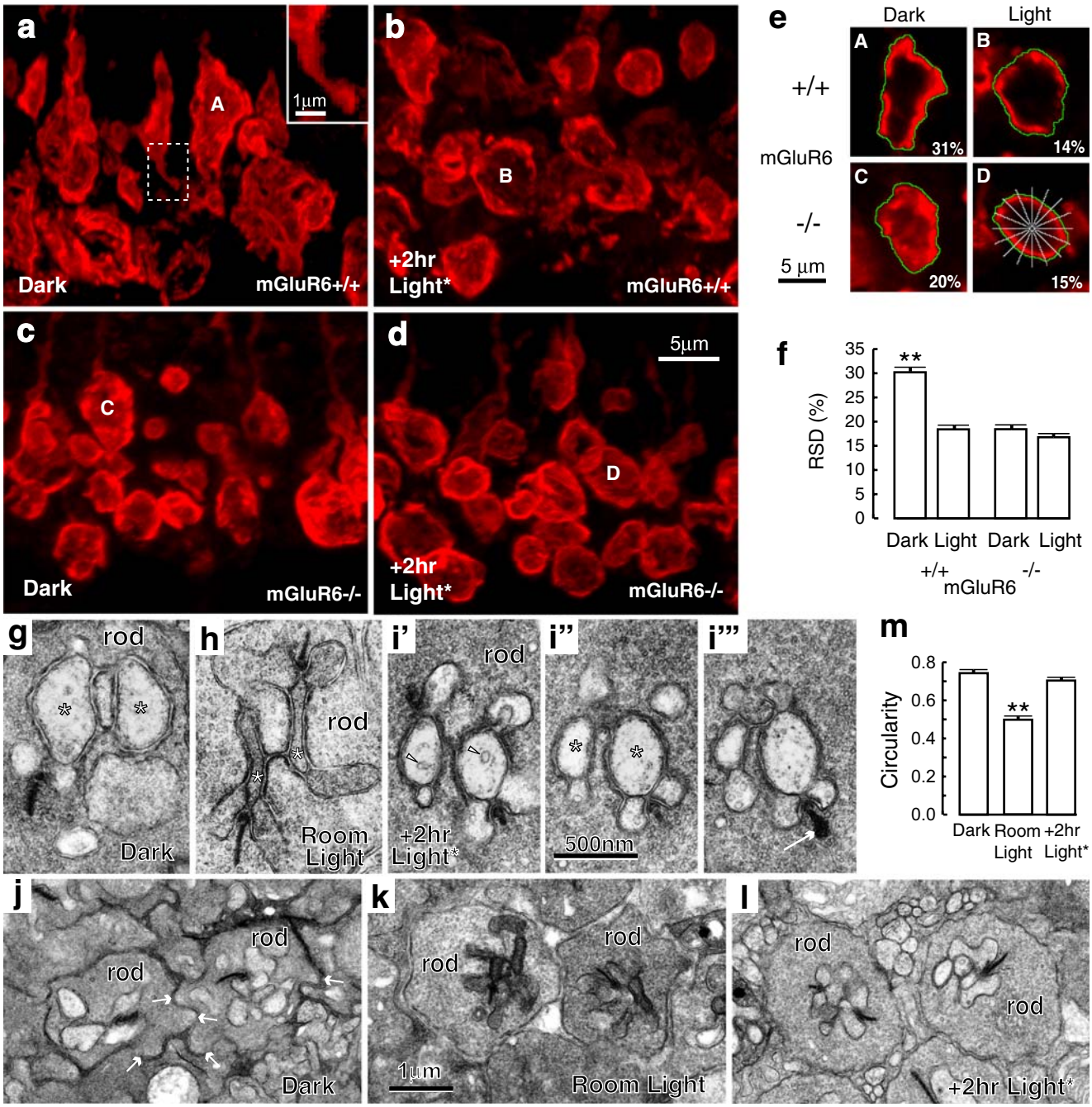

of the three other groups. The terminal swellings in both enhanced-light- and dark-adapted mGluR6-deficient retinas were as round (17%–18%) as those in enhanced-light-adapted wild-type retinas (18%), in marked contrast to the terminal swellings in dark-adapted wild-type retinas (30%). These data are comparable to those obtained in goldfish mixed rod-cone bipolar cells (Job and Lagnado 1998).

The morphology of rod bipolar invaginating dendrites was examined by electron microscopy of serially cut, tangential sections (Fig. 7g, i) of dark- and enhanced-light-adapted retinas of wild-type mice at 10 weeks of age. Conventional room-light-adapted retinas of wild-type mice at 10 weeks of age (Fig. 7h) were also compared with dark- or enhanced-light-adapted retinas as controls for wild-type mice rod bipolar dendrites at 4 and 90 weeks of age (Fig. 6a, b, f). Unexpectedly, cross-sectional contours of invaginating dendrites of rod bipolar cells in dark-adapted retinas from wild-type mice just before dawn were ovoid with some irregularities and were not slit-like (Fig. 7g). The dendritic tips showed some swelling (Fig. 7g) in contrast to the axon terminals that were not round but elongated (Fig. 7a). Noticeably, the outer contours of the rod spherules

Fig. 7 Comparison of rod bipolar axon terminals from wild-type (+/+) and mGluR6-deficient (−/−) mice after dark and enhanced-light adaptation. **a**–**d** Stacked confocal fluorescent images of PKCα-immunolabeled rod bipolar axon terminals (13 superimposed optical sections; 100× objective; z-axis step=0.6 μm; total thickness=8 μm). **a**, **b** Axon terminals in dark-adapted wild-type (+/+) mouse retinas (n=3 mice) show elongated shrunken profiles with irregular surfaces. *Inset* A: small terminal bulb projection at the axonal tip (*boxed area* in **a**). **b** In contrast, axon terminals in enhanced-light-adapted wild-type (+/+) retinas (n=3 mice) have round contours. **c**, **d** In dark- and enhanced-light-adapted mGluR6-deficient (−/−) retinas (n=3 mice), axon terminals are as round as in enhanced-light-adapted wild-type (+/+) retinas (n=3 mice). **e** Contour profiles (*green*) in a single optical section of rod bipolar cell terminals are shown (*A-D* in **a**–**d**). The outer contour of each PKCα–immunolabeled terminal was obtained from its representative optical section. The radial standard deviation of each contour profile was computed as a percentage of the mean radial distance (16 *radial white dotted lines*). **f** Radial standard deviation of rod bipolar axon terminal contours in wild-type (+/+) and mGluR6-deficient (−/−) retinas under both dark and enhanced-light adaptation. $^{**}P<0.0001$ compared with three other groups, Tukey-Kramer's test, n=90/group. **g-i** Electron micrographs of rod photoreceptor spherules in cross sections of dark-adapted (**g**, **j**), room-light-adapted (**h**, **k** ~500 lux) and enhanced-light-adapted (**i**, **l** ~500 lux plus 2 h at 2000 lux) retinas. All synaptic ribbons in the rod cytoplasm faced a postsynaptic triad (rod bipolar invaginating dendrite and two horizontal cell processes; *stars* rod bipolar invaginating dendrite). Note the vesicle and small vacuole in the bipolar cell cytoplasm (*arrowheads* in **i'**) and the club-shaped ribbon (*long arrow* in **i'"**). The outer contours of dark-adapted rod spherules are markedly wavy (*short arrows* in **j**). **m** Circularity of the cross-sectional contours of invaginating dendrites of rod bipolar cells. $^{**}P<0.0001$ compared with two other groups, Tukey-Kramer's test, n=60/group

were also conspicuously undulated in dark-adapted retinas (Fig. 7j) as compared with room-light-adapted (Fig. 7k) or enhanced-light-adapted (Fig. 7l) retinas. In contrast, the contours of the invaginating dendrites in room-light-adapted retinas from wild-type mice were slit-like (Fig. 7h) as expected (Fig. 6a, b). The shape of invaginating dendrites did not differ greatly with age (4, 10, and 90 weeks) in room-light-adapted retinas from wild-type mice (P=0.056 for 4 and 90 weeks; P=0.75 for 10 and 90 weeks, one-way ANOVA followed by Tukey-Kramer's test, n=60 dendrites/group). In the enhanced-light-adapted retinas from wild-type mice, however, club-shaped synaptic ribbons were observed at the rod photoreceptor terminals (Fig. 7i'"), and rod bipolar invaginating dendrites were generally ovoid with variable degrees of roundness (Fig. 7i', i'', i'"). This ovoid shape of the invaginating dendrites was similar to that observed in mGluR6-deficient mice (Fig. 6c, d). The circularity of the invaginating dendrites from wild-type mice was not statistically different after 2 h of additional intense illumination (0.70±0.02) or in darkness (0.74±0.02, P=0.41, one-way ANOVA followed by Tukey-Kramer's test, n=60 dendrites/group) but was significantly greater than that under room light (0.50±0.02, $^{**}P<0.0001$, one-way ANOVA followed by Tukey-Kramer's test, n=60 dendrites/group; Fig. 7m). However, the circularity of the invaginating dendrites in wild-type mice under enhanced-light adaptation (0.70±0.02) was significantly lower than that in mGluR6-deficient mice under room-light adaptation (0.85±0.01, 4 weeks; 0.79±0.01, 90 weeks; $^{**}P<0.0001$, one-way ANOVA followed by Tukey-Kramer's test, n=90 dendrites/group; Fig. 6f).

The shape similarity in rod bipolar axon terminals and invaginating dendrites from enhanced-light-adapted wild-type mice and from dark- and light-adapted mGluR6-deficient mice suggested that similar factors might affect cellular morphology. Therefore, we examined the invaginating dendrites of rod bipolar cells from enhanced-light-adapted wild-type retinas to determine whether ectopic ribbons were present. The dendrites contained vesicles and vacuoles of variable sizes and shapes (Fig. 7i') and cytoskeletal filamentous material. A series of 50 consecutive sections from three animals were imaged at ×3000 magnification (n=300–350 rod spherules). Relatively large, electron-dense bodies located in the invaginating dendrites were examined as candidate ectopic ribbons. Candidate ectopic ribbons were further examined at ×20,000 magnification to determine whether they were ectopic ribbons. No ectopic ribbons were found in any of the spherules examined (~1000 spherules, n=3 mice).

Discussion

A number of significant new findings have been made during this study. Ectopic ribbons have been observed in rod and ON-cone bipolar cells in mGluR6-deficient but not wild-type mice. The number of ectopic ribbons seen in rod bipolar cells increases during early growth but shows a ceiling effect. Polymorphic ectopic ribbons in rod bipolar cells of mGluR6-deficient mice are immunopositive for ribbon-specific RIBEYE protein and are often surrounded by a halo of vesicles immunonegative for synaptophysin. Ectopic ribbons have also been found in OFF-cone bipolar cell dendrites in both wild-type and mGluR6-deficient mouse retinas, but only in T2-type of the four OFF-bipolar cell types. T2 cells have more ribbon synapses and thicker axons than T1, T3, or T4 cells. Invaginating dendrites and axon terminals of mGluR6-deficient rod bipolar cells are rounder than those of wild-type bipolar cells. Wild-type mice under enhanced-light adaptation also have rounder invaginating dendrites and axon terminals than those under room-light adaptation, but no detectable ectopic ribbons (Fig. 8).

Cellular activities correlated with ectopic distribution of ribbons

ON- and OFF-bipolar cells differ in their dendritic intracellular signaling cascades (Nawy and Jahr 1990; Shiells and Falk 1990; Kaneko 1999). ON-bipolar cells depolarize via

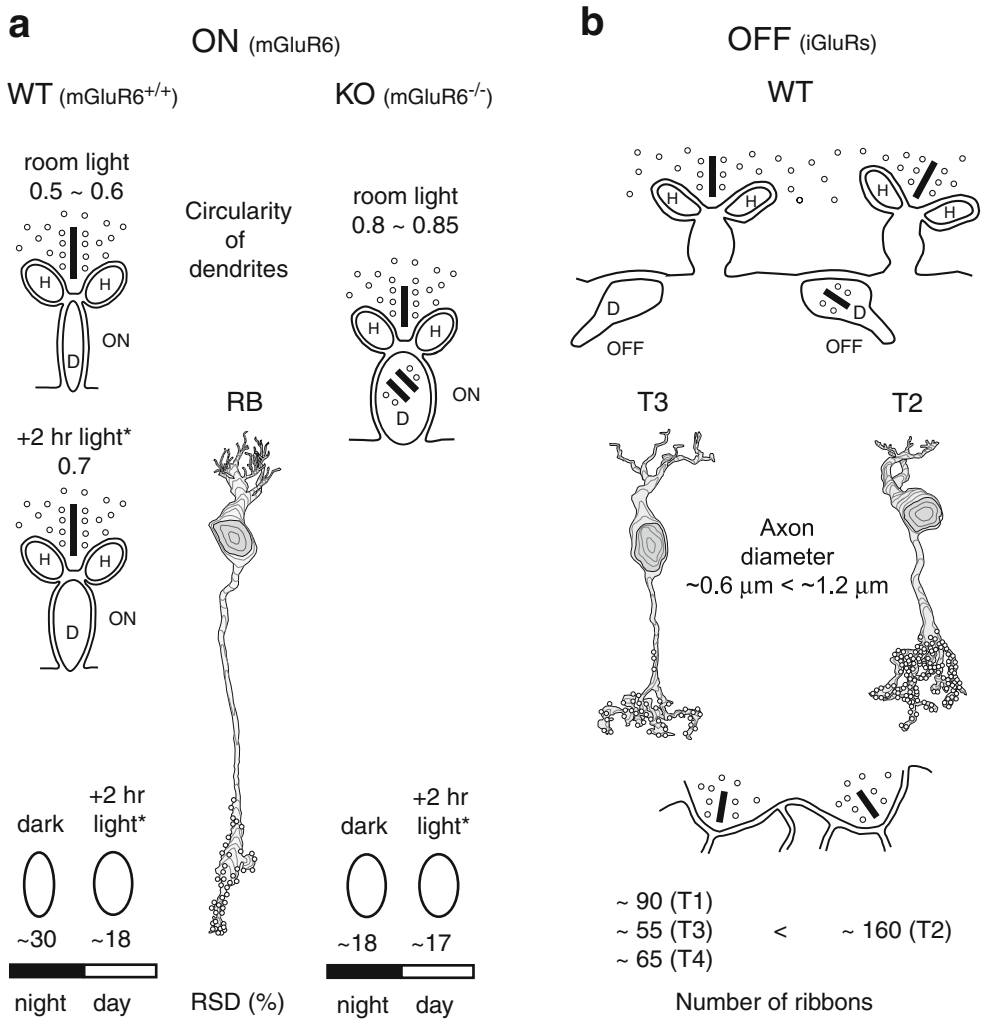

Fig. 8 Representations of ectopic ribbons in dendrites (*D*) of mGluR6-deficient (*KO*) rod bipolar (*RB*) cells and wild-type (*WT*) OFF-cone bipolar cells. Horizontal cells (*H*) are also depicted. **a** Ectopic ribbons are found in dendrites of KO RB cells but not in WT RB cells. Invaginating dendrites and axon terminals of KO RB cells are rounder than WT RB cells when mice are exposed to a daily cycle of dark and room light. However, the roundness (*RSD*) of invaginating dendrites and axon terminals of WT RB cells depends on light exposure, becoming rounder with exposure to 2 h (*+2 hr light**) of intense illumination. **b** Ectopic ribbons are found in dendrites of T2 OFF-bipolar cells, which possess two- to three-fold more synaptic ribbons and two-fold thicker axon cylinders than T1, T3, or T4 cells (*iGluRs* ionotropic glutamate receptors)

sign-inverting synapses that open cation channels at the dendrite in response to light (Berntson and Taylor 2000; Euler and Masland 2000). Conversely, OFF-bipolar cells, which are known to express ionotropic glutamate receptors (iGluRs) at the dendrite, hyperpolarize via sign-conserving synapses that close cation channels (DeVries and Schwartz 1999). However, both ON- and OFF-bipolar axon terminals release glutamate at their ribbon synapses in a similar depolarization-dependent manner (Tachibana 1999).

mGluR6 is a $G\alpha_o$-protein-linked glutamate receptor expressed exclusively in the dendrites of rod and ON-cone bipolar cells (Nakanishi 1994) and has a sign-inverting effect resulting in membrane hyperpolarization in response to glutamate. Ablation of the *mGluR6* gene results in a complete loss of *mGluR6* mRNA and mGluR6 immunoreactivity in ON-type bipolar cells (Masu et al. 1995). Electroretinogram analysis and recordings from the superior colliculus have indicated that mGluR6 deficiency abolishes ON responses without significant change in visual transmission of OFF responses (Masu et al. 1995). Thus, mGluR6-deficient ON-bipolar cells are considered to be continuously non-hyperpolarized even in darkness. This hypothesis is supported by a couple of developmental studies on retinas. The activation of mGluR6 by L-AP4 (glutamate analog), presumably by keeping the membrane potential hyperpolarized (Slaughter and Miller 1981), causes retardation of the dendritic segregation of the synaptically connected ON- and OFF-ganglion cells. This

morphological abnormality in the ganglion cells has been ascribed to the prolonged suppression of glutamate release from the hyperpolarized bipolar axon synaptic terminals (Bodnarenko and Chalupa 1993; Bodnarenko et al. 1995). On the other hand, deficiency of mGluR6 results in no difference compared with the wild-type mice in the stratification of ganglion cells. This is thought to be attributable to the lifelong activation of glutamate release from the non-hyperpolarized bipolar axon synaptic terminals (Tagawa et al. 1999). If glutamate is continuously released, vesicle replenishment from a cytoplasmic reserve pool of preformed vesicles becomes necessary for ribbon synapses to engage in indefatigable signaling (Gomis et al. 1999; Griesinger et al. 2005). When bipolar axon terminals require a greater replenishment of protein supply than that achieved by endocytic recycling, axonal transport may increase (von Gersdorff and Matthews 1997; Singer and Diamond 2006). Thus, ectopic ribbons might be correlated with the increase in intracellular transport of synaptic proteins.

Among the four types (T1–T4) of OFF-cone bipolar cells, only T2 cells have ectopic ribbons in their dendrites. T2 cells possess about two to three times more synaptic ribbons at the axon terminal. Sterling and Freed (2007) have suggested a strong correlation between the number of synaptic ribbons and the rate of quantal release of neurotransmitters in bipolar cells. The T2 cells also have axons about twice as thick as T1, T3, and T4 cells (Fig. 8b). These findings suggest that T2 cells support greater axonal transport of synaptic proteins than other bipolar cell types. Cells with more synaptic ribbons would require thicker axons, which may contain more axonal microtubules, which in turn may provide for increased levels of axonal transport.

Thus, intracellular transport for the replenishment of synaptic proteins may be a common underlying factor that gives rise to ectopic ribbon proteins in both ON- and OFF-bipolar cells. Microtubules with their intrinsic polarity and their specific motors have been established to serve as the infrastructure for polarized protein trafficking (Hirokawa and Takemura 2005). Recent studies have shown that axon-targeted proteins produced in the soma are transported mostly to the axon, but also to the dendrites. For example, Stowell and Craig (1999) have demonstrated, in cultured hippocampal neurons, that the C-terminal sequence in mGluR7 is the axonal targeting motif, although mGluR7 has also been detected in dendrites. In mGluR6-deficient mouse retinas, we have also found immunoreactivity for mGluR7 (generally localized at axon terminals of cone bipolar cells) in dendrites of ON-cone bipolar cells (Tsukamoto et al. 2007).

This ectopic trafficking of axonal proteins may occur because plus-end-distal microtubules are present both in the dendritic and axonal processes, whereas minus-end-distal microtubules are found only in dendritic processes (Baas et al. 1988). Since carriers of axon-targeted proteins are transported by plus-end directed motors, the carriers loaded with axon-targeted proteins can enter either the axon or dendrites via plus-end directed motors. When the transport of axon-targeted proteins increases, the amount of axon-targeted proteins inflowing into dendrites also increases. In addition, the ectopic proteins in dendrites are regulated not only by their inflow into dendrites, but also by their outflow from dendrites. If the inflow overwhelms the outflow, the axon-targeted protein may accumulate in dendrites.

To ensure the axonal localization of specific proteins, post-transport mechanisms are also required to exclude axon-targeted proteins from dendrites and concomitantly to allow their selective retention at axon terminals (Craig and Banker 1994; Burack et al. 2000; Garrido et al. 2001; Sampo et al. 2003). Most probably, ON- and OFF-bipolar dendrites give rise to different post-transport mechanisms, because they have different intracellular signaling cascades downstream of mGluR6 and iGluRs (Nakanishi 1992; Brandstätter et al. 1998; Yoshida et al. 1998; Higashida et al. 2003). This may be one of the reasons that mGluR7 is detected in mGluR6-deficient ON-cone bipolar dendrites, but not in those of OFF-cone bipolar cells, although the axonal targeting motif should not be any different. With the exclusion processes disrupted in mGluR6-deficient ON-cone bipolar dendrites, ectopic axonal proteins might readily accumulate. On the other hand, in OFF-cone bipolar dendrites with an intact exclusion system, the ectopic accumulation might depend more on the relative abundance of proteins at the axon terminal: the synaptic ribbon-component protein RIBEYE may be more abundant than the receptor protein mGluR7. Thus, RIBEYE or its ribbon-complex may more readily accumulate, via intracellular transport, in the OFF-cone bipolar dendrites, whereas mGluR7 does not. Further experiments are necessary to determine the signaling cascades contributing to and influencing the balance in the inflow-outflow of ectopic axonal proteins in dendrites.

Ectopic ribbon deformity and synaptophysin

Synaptic ribbons, as part of the cytomatrix of the presynaptic active zone (Dick et al. 2003; Takao-Rikitsu et al. 2004), tether synaptic vesicles (Sterling and Matthews 2005). Dimers of RIBEYE molecules are polymerized into plates, two forming a bi-laminate structure (Schmitz et al. 2000). Ectopic ribbons, however, are deformed in both mGluR6-deficient rod and ON-cone bipolar cell dendrites. The ectopic ribbons often consist of two curved plates with an inner space and are free-floating in the dendritic cytoplasm.

RIBEYE alone is known to be insufficient to organize ribbons. At least one additional inner-core protein is required, and other accessory proteins are also involved in

ribbon organization (Schmitz et al. 2000). If inner-core and accessory proteins are transported to the dendrites by carriers different from those transporting RIBEYE protein, dendritic compartments may lack some of the proteins required for ribbon organization, thereby resulting in deformed ectopic ribbons. Dick et al. (2003) have shown that the absence of Bassoon protein in mutant mice prevents the anchoring of the photoreceptor ribbon to the presynaptic active zone resulting in freely floating ectopic ribbons in the terminal cytoplasm. As bipolar cell ribbon synapses also contain Bassoon protein (Deguchi-Tawarada et al. 2006), free-floating ectopic ribbons in bipolar dendrites may arise because of a lack of Bassoon protein.

Synaptophysin has not been detected in the synaptic-like vesicles associated with ectopic ribbons, exemplifying that not all axonal proteins are ectopically distributed to dendrites. It is known that the newly synthesized synaptophysin in PC12 cells shuttles between the cell surface and intracellular membranes before delivery to target sites (Régnier-Vigouroux et al. 1991; De Camilli et al. 2001). Such a unique transport mechanism may partially explain the difference in synaptophysin distribution from that of RIBEYE and mGluR7. Thus the deformity in ectopic ribbons and the lack of ectopic distribution of synaptophysin might also be attributable to intracellular transport.

Enhanced-light adaptation and mGluR6 deficiency

To address whether "enhanced-light" adaptation simulates the mGluR6-deficient state of the morphological changes in axon terminals of rod bipolar cells, we have compared the dark and enhanced-light adaptations in both wild-type and mGluR6-deficient mice. Rod bipolar axon terminals with their many ribbon synapses are likely to be affected by the balance between exocytosis and endocytosis but are relatively free from spatial restrictions by other impinging cells. The round contour of rod bipolar axon terminals in both dark- and light-adapted mGluR6-deficient mice is similar in size and shape to that of enhanced-light-adapted wild-type mice (RSD: ~18 and ~17 vs. ~18, respectively; Fig. 8a). Intense illumination is thought to discontinue glutamate release from rods, thus depolarizing rod bipolar cells and resulting in increased inflow of calcium ions at their axon terminals (Berntson and Taylor 2000; Euler and Masland 2000). If the rate of Ca^{2+}-triggered exocytosis is greater than the rate of endocytosis, the terminal contour might become enlarged and rounder. The formation of actin filaments (Job and Lagnado 1998) might also contribute to the rearrangement of local cytoskeletal architecture. The same rationale can be applied to mGluR6-deficient rod bipolar axon terminals, assuming that the mGluR6-deficient rod bipolar cells keep releasing glutamate at a higher rate of exocytosis than the dark-adapted wild-type rod bipolar cells.

Unlike the axon terminals, the invaginating dendrites of rod bipolar cells do not undergo exocytosis and endocytosis. At the photoreceptor ribbon synapses, the rod spherules undergo light-dependent exocytosis and endocytosis. Therefore, the finding that rod bipolar invaginating dendrites are rounder in dark-adapted retinas than in room-light-adapted wild-type retinas (circularity: 0.74 vs. 0.5–0.6, respectively; Figs. 6f, 7m) is unexpected. Since this phenomenon shows a discrepancy with the slenderness of dark-adapted rod bipolar axon terminals, some dendrite-specific factors might be involved in the shaping of the invaginating dendrites of dark-adapted rod bipolar cells. The rod bipolar invaginating dendrites, which are spatially restricted by the rod photoreceptor basal membrane, may be indirectly affected by lighting conditions via the shape change in the rod basal membrane. Several researchers have reported unique structural changes in rod and cone photoreceptor terminals under dark and light adaptations (Cragg 1969; Schaeffer and Raviola 1978; Cooper and McLaughlin 1982; Brandon and Lam 1983). For example, Schaeffer and Raviola (1978) have shown, in turtle retinas, that neural processes (bipolar and horizontal) in contact with cone photoreceptor cells at invaginating synapses penetrate more deeply into the pedicle in dark-adapted retinas than in light-adapted retinas. The authors suggest that the shape change reflects an imbalance between exocytosis and endocytosis at the cone terminal as the rate of vesicle fusion increases in darkness. A similar expansion of rod terminal membrane has also been observed in our dark-adapted mouse retinas (Fig. 7j). The increased circularity of the dendritic contour might be shaped by both membranes of the rod terminal and the rod bipolar invaginating dendrites, which are in apposition to each other.

Rod bipolar invaginating dendrites were more circular in enhanced-light-adapted wild-type than in room-light-adapted wild-type retinas (circularity: 0.7 vs. 0.5–0.6, respectively; Fig. 8a). The osmotic pressure attributable to the depolarization-dependent inflow of cations might be a major factor in this circularity, although further experiments are needed to verify this possibility (Somero and Yancey 1997; Lang et al. 1998). The same rationale can be applied to mGluR6-deficient rod bipolar invaginating dendrites (0.8–0.85), assuming that many cation channels are open at the membrane of mGluR6-deficient rod bipolar dendrites because of null glutamate input.

Despite the similarity in contour roundness in the axon terminal (RSD: ~18 vs. ~17, respectively), the circularity in the invaginating dendrites of rod bipolar cells in enhanced-light-adapted wild-type retinas is significantly smaller than that in mGluR6-deficient retinas (circularity: 0.7 vs. 0.8–0.85, respectively; Fig. 8a). Possibly, the enhanced-light adaptation protocol in wild-types does not fully simulate mGluR6-deficient rod bipolar invaginating dendrites. A number of factors may account for the difference between

enhanced-light-adapted wild-type and mGluR6-deficient retinas. Most importantly, mGluR6 deficiency is a permanent genetic condition, whereas light adaptation is a temporary physiological condition in response to light stimuli. This notable difference may also account for the absence of ectopic ribbons in the one thousand spherules examined in wild-type retinas under enhanced-light adaptation. Further experiments are needed to explore other factors involved in the difference between enhanced-light-adapted wild-type and mGluR6-deficient retinas in order to determine the way that the ectopic distributions are induced. In the present study, we have been unable to examine the effect of enhanced-light adaptation on the ectopic ribbons in the T2 OFF-cone bipolar dendrites because of limitations in our current research setup. This issue also remains to be pursued.

Concluding remarks

This study presents new observations regarding the distribution of ectopic ribbons in ON- and OFF-bipolar cells. The occurrence of ectopic ribbons depends on mGluR6 deficiency in rod and ON-cone bipolar cells, but on cell type in OFF-cone bipolar cells. Both ON- and OFF-bipolar cells are engaged in glutamate release at ribbon synapses from the axon terminal. The increased level of exocytosis at axon terminals similar to that in the enhanced-light-adapted state has been implicated in the function of mGluR6-deficient ON-bipolar cells. The numerous synapses and thick axons observed in T2 OFF-cone bipolar cells suggest a high rate of synaptic protein turnover. Thus, the intracellular transport for the replenishment of synaptic proteins might be one of the factors correlated with the occurrence of ectopic ribbons. This insight, based on a number of findings, will be useful for future studies to elucidate the synaptic protein trafficking downstream of the mGluR6 and iGluR signals.

Acknowledgements Our sincere thanks are extended to Dr. N. Vardi (Pennsylvania) for the EM samples of $G\alpha_o$-deficient mice, to Dr. Y. Muraoka for advice on statistics, to Drs. H. Sawai and T. Miyoshi for their critical reading of the manuscript, to Ms. K. Iseki for animal care, and to Ms. N. Omi and Ms T. Inoue for their technical assistance.

References

Baas PW, Deitch JS, Black MM, Banker GA (1988) Polarity orientation of microtubules in hippocampal neurons: uniformity in the axon and nonuniformity in the dendrite. Proc Natl Acad Sci USA 85:8335–8339

Behrens UD, Wagner HJ (1996) Adaptation-dependent changes of bipolar cell terminals in fish retina: effects on overall morphology and spinule formation in Ma and Mb cells. Vision Res 36:3901–3911

Behrens UD, Kasten P, Wagner HJ (1998) Adaptation-dependent plasticity of rod bipolar cell axon terminal morphology in the rat retina. Cell Tissue Res 294:243–251

Behrens UD, Douglas RH, Sugden D, Davies DJ, Wagner HJ (2000) Effect of melatonin agonists and antagonists on horizontal cell spinule formation and dopamine release in a fish retina. Cell Tissue Res 299:299–306

Berntson A, Taylor WR (2000) Response characteristics and receptive field widths of on-bipolar cells in the mouse retina. J Physiol (Lond) 524:879–889

Blanks JC, Adinolfi AM, Lolley RN (1974) Synaptogenesis in the photoreceptor terminal of the mouse retina. J Comp Neurol 156:81–93

Bodnarenko SR, Chalupa LM (1993) Stratification of ON and OFF ganglion cell dendrites depends on glutamate-mediated afferent activity in the developing retina. Nature 364:144–146

Bodnarenko SR, Jeyarasasingam G, Chalupa LM (1995) Development and regulation of dendritic stratification in retinal ganglion cells by glutamate-mediated afferent activity. J Neurosci 15:7037–7045

Brandon C, Lam DM (1983) The ultrastructure of rat rod synaptic terminals: effects of dark-adaptation. J Comp Neurol 217:167–175

Brandstätter JH, Koulen P, Wässle H (1998) Diversity of glutamate receptors in the mammalian retina. Vision Res 38:1385–1397

Burack MA, Silverman MA, Banker G (2000) The role of selective transport in neuronal protein sorting. Neuron 26:465–472

Cooper NG, McLaughlin BJ (1982) Structural correlates of physiological activity in chick photoreceptor synaptic terminals: effects of light and dark stimulation. J Ultrastruct Res 79:58–73

Cragg BG (1969) Structural changes in naive retinal synapses detectable within minutes of first exposure to daylight. Brain Res 15:79–96

Craig AM, Banker G (1994) Neuronal polarity. Annu Rev Neurosci 17:267–310

De Camilli P, Slepnev VI, Shupliakov O, Brodin L (2001) Synaptic vesicle endocytosis. In: Cowan WM, Sudhof TC, Stevens CF, Davies K (eds) Synapses. Johns Hopkins University Press, Baltimore, pp 217–274

Deguchi-Tawarada M, Inoue E, Takao-Rikitsu E, Inoue M, Kitajima I, Ohtsuka T, Takai Y (2006) Active zone protein CAST is a component of conventional and ribbon synapses in mouse retina. J Comp Neurol 495:480–496

DeVries SH, Schwartz EA (1999) Kainate receptors mediate synaptic transmission between cones and "Off" bipolar cells in a mammalian retina. Nature 397:157–160

Dhingra A, Lyubarsky A, Jiang M, Pugh EN Jr, Birnbaumer L, Sterling P, Vardi N (2000) The light response of ON bipolar neurons requires G[alpha]o. J Neurosci 20:9053–9058

Dhingra A, Jiang M, Wang TL, Lyubarsky A, Savchenko A, Bar-Yehuda T, Sterling P, Birnbaumer L, Vardi N (2002) Light response of retinal ON bipolar cells requires a specific splice variant of Galpha(o). J Neurosci 22:4878–4884

Dick O, tom Dieck S, Altrock WD, Ammermuller J, Weiler R, Garner CC, Gundelfinger ED, Brandstätter JH (2003) The presynaptic active zone protein bassoon is essential for photoreceptor ribbon synapse formation in the retina. Neuron 37:775–786

Dowling JE (1987) The retina. Harvard University Press, Cambridge, Mass.

Euler T, Masland RH (2000) Light-evoked responses of bipolar cells in a mammalian retina. J Neurophysiol 83:1817–1829

Fisher LJ (1979) Development of synaptic arrays in the inner plexiform layer of neonatal mouse retina. J Comp Neurol 187:359–372

Garrido JJ, Fernandes F, Giraud P, Mouret I, Pasqualini E, Fache MP, Jullien F, Dargent B (2001) Identification of an axonal determinant in the C-terminus of the sodium channel Na(v)1.2. EMBO J 20:5950–5961

Ghosh KK, Bujan S, Haverkamp S, Feigenspan A, Wässle H (2004) Types of bipolar cells in the mouse retina. J Comp Neurol 469:70–82

Gomis A, Burrone J, Lagnado L (1999) Two actions of calcium regulate the supply of releasable vesicles at the ribbon synapse of retinal bipolar cells. J Neurosci 19:6309–6317

Griesinger CB, Richards CD, Ashmore JF (2005) Fast vesicle replenishment allows indefatigable signalling at the first auditory synapse. Nature 435:212–215

Higashida H, Zhang JS, Mochida S, Chen XL, Shin Y, Noda M, Hossain KZ, Hoshi N, Hashii M, Shigemoto R, Nakanishi S, Fukuda Y, Yokoyama S (2003) Subtype-specific coupling with ADP-ribosyl cyclase of metabotropic glutamate receptors in retina, cervical superior ganglion and NG108-15 cells. J Neurochem 85:1148–1158

Hirokawa N, Takemura R (2005) Molecular motors and mechanisms of directional transport in neurons. Nat Rev Neurosci 6:201–214

Ivanova E, Müller U, Wässle H (2006) Characterization of the glycinergic input to bipolar cells of the mouse retina. Eur J Neurosci 23:350–364

Job C, Lagnado L (1998) Calcium and protein kinase C regulate the actin cytoskeleton in the synaptic terminal of retinal bipolar cells. J Cell Biol 143:1661–1672

Kaneko A (1999) Responses of bipolar cells: on and off pathways. In: Toyoda J, Murakami M, Kaneko A, Saito T (eds) The retinal basis of vision. Elsevier Science, Amsterdam, pp 103–114

Kolb H (1977) The organization of the outer plexiform layer in the retina of the cat: electron microscopic observations. J Neurocytol 6:131–153

Kosaka J, Suzuki A, Morii E, Nomura S (1998) Differential localization and expression of alpha and beta isoenzymes of protein kinase C in the rat retina. J Neurosci Res 54:655–663

Lang F, Lepple-Wienhues A, Szabo I, Siemen D, Gulbins E (1998) Cell volume in cell proliferation and apoptotic cell death. Contrib Nephrol 123:158–168

Linberg KA, Fisher SK (1988) Ultrastructural evidence that horizontal cell axon terminals are presynaptic in the human retina. J Comp Neurol 268:281–297

Masu M, Iwakabe H, Tagawa Y, Miyoshi T, Yamashita M, Fukuda Y, Sasaki H, Hiroi K, Nakamura Y, Shigemoto R, Takada M, Nakamura K, Nakao K, Katsuki M, Nakanishi S (1995) Specific deficit of the ON response in visual transmission by targeted disruption of the mGluR6 gene. Cell 80:757–765

Nakanishi S (1992) Molecular diversity of glutamate receptors and implications for brain function. Science 258:597–603

Nakanishi S (1994) Metabotropic glutamate receptors: synaptic transmission, modulation, and plasticity. Neuron 13:1031–1037

Nawy S, Jahr CE (1990) Suppression by glutamate of cGMP-activated conductance in retinal bipolar cells. Nature 346:269–271

Nomura A, Shigemoto R, Nakamura Y, Okamoto N, Mizuno N, Nakanishi S (1994) Developmentally regulated postsynaptic localization of a metabotropic glutamate receptor in rat rod bipolar cells. Cell 77:361–369

Régnier-Vigouroux A, Tooze SA, Huttner WB (1991) Newly synthesized synaptophysin is transported to synaptic-like microvesicles via constitutive secretory vesicles and the plasma membrane. EMBO J 10:3589–3601

Sampo B, Kaech S, Kunz S, Banker G (2003) Two distinct mechanisms target membrane proteins to the axonal surface. Neuron 37:611–624

Sassoè-Pognetto M, Wässle H, Grünert U (1994) Glycinergic synapses in the rod pathway of the rat retina: cone bipolar cells express the alpha 1 subunit of the glycine receptor. J Neurosci 14:5131–5146

Sawada H, Esaki M (2002) Pre-embedding immunoelectron microscopy with nanogold immunolabeling, silver enhancement, and its stabilization by gold. In: Hacker GW, Gu J (eds) Gold and silver staining: techniques in molecular morphology. CRC Press, Boca Raton, pp 169–176

Schaeffer SF, Raviola E (1978) Membrane recycling in the cone cell endings of the turtle retina. J Cell Biol 79:802–825

Schmitz F, Konigstorfer A, Südhof TC (2000) RIBEYE, a component of synaptic ribbons: a protein's journey through evolution provides insight into synaptic ribbon function. Neuron 28:857–872

Shiells RA, Falk G (1990) Glutamate receptors of rod bipolar cells are linked to a cyclic GMP cascade via a G-protein. Proc Biol Sci 242:91–94

Singer JH, Diamond JS (2006) Vesicle depletion and synaptic depression at a mammalian ribbon synapse. J Neurophysiol 95:3191–3198

Slaughter MM, Miller RF (1981) 2-Amino-4-phosphonobutyric acid: a new pharmacological tool for retina research. Science 211:182–185

Somero GN, Yancey PH (1997) Osmolytes and cell volume regulation: physiological and evolutionary principles. In: Hoffman JF, Jamieson JD (eds) Handbook of Physiology, section 14. Oxford University Press, New York, pp 441–484

Specht D, tom Dieck S, Ammermüller J, Regus-Leidig H, Gundelfinger ED, Brandstätter JH (2007) Structural and functional remodeling in the retina of a mouse with a photoreceptor synaptopathy: plasticity in the rod and degeneration in the cone system. Eur J Neurosci 26:2506–2515

Spiwoks-Becker I, Lasarzik I, Vollrath L (2000) Transient synaptic ribbons in the mammalian retina at unusual sites. J Neurocytol 29:81–89

Sterling P, Freed M (2007) How robust is a neural circuit? Vis Neurosci 24:563–571

Sterling P, Matthews G (2005) Structure and function of ribbon synapses. Trends Neurosci 28:20–29

Stowell JN, Craig AM (1999) Axon/dendrite targeting of metabotropic glutamate receptors by their cytoplasmic carboxy-terminal domains. Neuron 22:525–536

Tachibana M (1999) Regulation of transmitter release from retinal bipolar cells. Prog Biophys Mol Biol 72:109–133

Tagawa Y, Sawai H, Ueda Y, Tauchi M, Nakanishi S (1999) Immunohistological studies of metabotropic glutamate receptor subtype 6-deficient mice show no abnormality of retinal cell organization and ganglion cell maturation. J Neurosci 19:2568–2579

Takao-Rikitsu E, Mochida S, Inoue E, Guchi-Tawarada M, Inoue M, Ohtsuka T, Takai Y (2004) Physical and functional interaction of the active zone proteins, CAST, RIM1, and Bassoon, in neurotransmitter release. J Cell Biol 164:301–311

tom Dieck S, Brandstätter JH (2006) Ribbon synapses of the retina. Cell Tissue Res 326:339–346

tom Dieck S, Altrock WD, Kessels MM, Qualmann B, Regus H, Brauner D, Fejtova A, Bracko O, Gundelfinger ED, Brandstätter JH (2005) Molecular dissection of the photoreceptor ribbon synapse: physical interaction of Bassoon and RIBEYE is essential for the assembly of the ribbon complex. J Cell Biol 168:825–836

Tsukamoto Y, Morigiwa K, Takao M, Fukuda Y (1999) Ectopic expression of presynaptic structures in the postsynaptic dendrites of rod bipolar cells in mouse retinas deficient in metabotropic glutamate receptor subtype 6 (mGluR6). Abstracts Soc Neurosci 25:136

Tsukamoto Y, Morigiwa K, Ueda M, Sterling P (2001) Microcircuits for night vision in mouse retina. J Neurosci 21:8616–8623

Tsukamoto Y, Morigiwa K, Ishii M, Takao M, Iwatsuki K, Nakanishi S, Fukuda Y (2007) A novel connection between rods and ON cone bipolar cells revealed by ectopic metabotropic glutamate receptor 7 (mGluR7) in mGluR6-deficient mouse retinas. J Neurosci 27:6261–6267

Ueda Y, Iwakabe H, Masu M, Suzuki M, Nakanishi S (1997) The mGluR6 5' upstream transgene sequence directs a cell-specific and developmentally regulated expression in retinal rod and ON-type cone bipolar cells. J Neurosci 17:3014–3023

Vardi N, Morigiwa K (1997) ON cone bipolar cells in rat express the metabotropic receptor mGluR6. Vis Neurosci 14:789–794

Vollrath L, Spiwoks-Becker I (1996) Plasticity of retinal ribbon synapses. Microsc Res Tech 35:472–487

von Gersdorff H, Matthews G (1997) Depletion and replenishment of vesicle pools at a ribbon-type synaptic terminal. J Neurosci 17:1919–1927

Wagner HJ (1997) Presynaptic bodies ("ribbons"): from ultrastructural observations to molecular perspectives. Cell Tissue Res 287:435–446

Wagner HJ, Djamgoz MB (1993) Spinules: a case for retinal synaptic plasticity. Trends Neurosci 16:201–206

Wagner HJ, Kröger RH (2005) Adaptive plasticity during the development of colour vision. Prog Retin Eye Res 24:521–536

Wiedenmann B, Franke WW (1985) Identification and localization of synaptophysin, an integral membrane glycoprotein of Mr 38,000 characteristic of presynaptic vesicles. Cell 41:1017–1028

Yazulla S, Studholme KM (1992) Light-dependent plasticity of the synaptic terminals of Mb bipolar cells in goldfish retina. J Comp Neurol 320:521–530

Yoshida K, Imaki J, Okamoto Y, Iwakabe H, Fujisawa H, Matsuda A, Nakanisi S, Matsuda H, Hagiwara M (1998) CREB-induced transcriptional activation depends on mGluR6 in rod bipolar cells. Brain Res Mol Brain Res 57:241–247